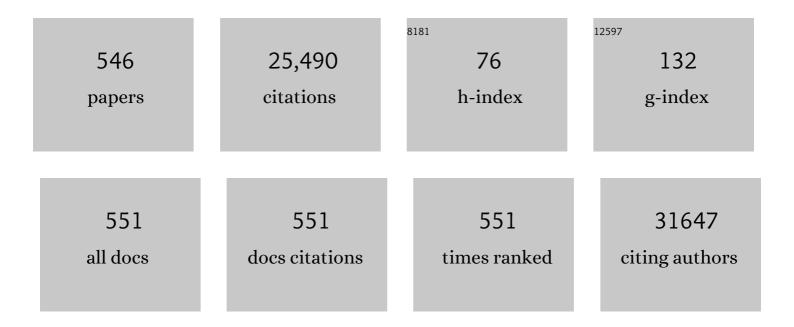
Chun-Li Wang

List of Publications by Year in descending order

Source: https://exaly.com/author-pdf/2212032/publications.pdf Version: 2024-02-01



#	Article	IF	CITATIONS
1	Mesoporous Silicaâ€Coated Gold Nanorods as a Lightâ€Mediated Multifunctional Theranostic Platform for Cancer Treatment. Advanced Materials, 2012, 24, 1418-1423.	21.0	881
2	Binding of blood proteins to carbon nanotubes reduces cytotoxicity. Proceedings of the National Academy of Sciences of the United States of America, 2011, 108, 16968-16973.	7.1	839
3	Effect of aspect ratio and surface defects on the photocatalytic activity of ZnO nanorods. Scientific Reports, 2014, 4, 4596.	3.3	761
4	Surface chemistry and aspect ratio mediated cellular uptake of Au nanorods. Biomaterials, 2010, 31, 7606-7619.	11.4	613
5	Bismuth Sulfide Nanorods as a Precision Nanomedicine for <i>in Vivo</i> Multimodal Imaging-Guided Photothermal Therapy of Tumor. ACS Nano, 2015, 9, 696-707.	14.6	503
6	Selective Targeting of Gold Nanorods at the Mitochondria of Cancer Cells: Implications for Cancer Therapy. Nano Letters, 2011, 11, 772-780.	9.1	475
7	Metal Organic Frameworks Route to <i>in Situ</i> Insertion of Multiwalled Carbon Nanotubes in Co ₃ O ₄ Polyhedra as Anode Materials for Lithium-Ion Batteries. ACS Nano, 2015, 9, 1592-1599.	14.6	462
8	Cytotoxic Potential of Silver Nanoparticles. Yonsei Medical Journal, 2014, 55, 283.	2.2	340
9	Covalently Attached Liquids: Instant Omniphobic Surfaces with Unprecedented Repellency. Angewandte Chemie - International Edition, 2016, 55, 244-248.	13.8	299
10	Abnormally enhanced thermoelectric transport properties of SWNT/PANI hybrid films by the strengthened PANI molecular ordering. Energy and Environmental Science, 2014, 7, 3801-3807.	30.8	285
11	Surface-Engineered Gold Nanorods: Promising DNA Vaccine Adjuvant for HIV-1 Treatment. Nano Letters, 2012, 12, 2003-2012.	9.1	282
12	Controlling Assembly of Paired Gold Clusters within Apoferritin Nanoreactor for in Vivo Kidney Targeting and Biomedical Imaging. Journal of the American Chemical Society, 2011, 133, 8617-8624.	13.7	258
13	Use of Synchrotron Radiation-Analytical Techniques To Reveal Chemical Origin of Silver-Nanoparticle Cytotoxicity. ACS Nano, 2015, 9, 6532-6547.	14.6	246
14	Hierarchical NiFe ₂ O ₄ /Fe ₂ O ₃ nanotubes derived from metal organic frameworks for superior lithium ion battery anodes. Journal of Materials Chemistry A, 2014, 2, 8048-8053.	10.3	240
15	Revealing the Binding Structure of the Protein Corona on Gold Nanorods Using Synchrotron Radiation-Based Techniques: Understanding the Reduced Damage in Cell Membranes. Journal of the American Chemical Society, 2013, 135, 17359-17368.	13.7	239
16	PANI/graphene nanocomposite films with high thermoelectric properties by enhanced molecular ordering. Journal of Materials Chemistry A, 2015, 3, 7086-7092.	10.3	224
17	ZnCl ₂ "Waterâ€inâ€Salt―Electrolyte Transforms the Performance of Vanadium Oxide as a Zn Battery Cathode. Advanced Functional Materials, 2019, 29, 1902653.	14.9	213
18	Full Assessment of Fate and Physiological Behavior of Quantum Dots Utilizing <i>Caenorhabditis elegans</i> as a Model Organism. Nano Letters, 2011, 11, 3174-3183.	9.1	212

#	Article	IF	CITATIONS
19	Na ₃ PSe ₄ : A Novel Chalcogenide Solid Electrolyte with High Ionic Conductivity. Advanced Energy Materials, 2015, 5, 1501294.	19.5	207
20	A high-rate aqueous rechargeable zinc ion battery based on the VS ₄ @rGO nanocomposite. Journal of Materials Chemistry A, 2018, 6, 23757-23765.	10.3	196
21	Carbon-Doped ZnO Nanostructures: Facile Synthesis and Visible Light Photocatalytic Applications. Journal of Physical Chemistry C, 2015, 119, 20544-20554.	3.1	193
22	Using Hollow Carbon Nanospheres as a Light-Induced Free Radical Generator To Overcome Chemotherapy Resistance. Journal of the American Chemical Society, 2015, 137, 1947-1955.	13.7	182
23	Phytic Acid-Assisted Formation of Hierarchical Porous CoP/C Nanoboxes for Enhanced Lithium Storage and Hydrogen Generation. ACS Nano, 2018, 12, 12238-12246.	14.6	175
24	Rapid Degradation and High Renal Clearance of Cu ₃ BiS ₃ Nanodots for Efficient Cancer Diagnosis and Photothermal Therapy <i>in Vivo</i> . ACS Nano, 2016, 10, 4587-4598.	14.6	173
25	Metal–organic framework derived Fe ₂ O ₃ @NiCo ₂ O ₄ porous nanocages as anode materials for Li-ion batteries. Nanoscale, 2014, 6, 5509-5515.	5.6	169
26	Gd-metallofullerenol nanomaterial as non-toxic breast cancer stem cell-specific inhibitor. Nature Communications, 2015, 6, 5988.	12.8	164
27	Vacancyâ€Contained Tetragonal Na ₃ SbS ₄ Superionic Conductor. Advanced Science, 2016, 3, 1600089.	11.2	163
28	Liquidâ€Exfoliated Black Phosphorous Nanosheet Thin Films for Flexible Resistive Random Access Memory Applications. Advanced Functional Materials, 2016, 26, 2016-2024.	14.9	161
29	Intracellular dynamics of cationic and anionic polystyrene nanoparticles without direct interaction with mitotic spindle and chromosomes. Biomaterials, 2011, 32, 8291-8303.	11.4	160
30	Fast intracellular dissolution and persistent cellular uptake of silver nanoparticles in CHO-K1 cells: implication for cytotoxicity. Nanotoxicology, 2015, 9, 181-189.	3.0	159
31	Anisotropic giant magnetoresistance in NbSb2. Scientific Reports, 2014, 4, 7328.	3.3	158
32	Interaction of gold nanoparticles with proteins and cells. Science and Technology of Advanced Materials, 2015, 16, 034610.	6.1	149
33	Controlled Incorporation of Ni(OH) ₂ Nanoplates Into Flowerlike MoS ₂ Nanosheets for Flexible Allâ€&olidâ€&tate Supercapacitors. Advanced Functional Materials, 2014, 24, 6700-6707.	14.9	145
34	Surface chemistry of gold nanorods: origin of cell membrane damage and cytotoxicity. Nanoscale, 2013, 5, 8384.	5.6	141
35	Electrolyte Engineering Enables High Stability and Capacity Alloying Anodes for Sodium and Potassium Ion Batteries. ACS Energy Letters, 2020, 5, 766-776.	17.4	134
36	Meso-scale oriented simulation towards virtual process engineering (VPE)—The EMMS Paradigm. Chemical Engineering Science, 2011, 66, 4426-4458.	3.8	130

#	Article	IF	CITATIONS
37	Novel Insights into Combating Cancer Chemotherapy Resistance Using a Plasmonic Nanocarrier: Enhancing Drug Sensitiveness and Accumulation Simultaneously with Localized Mild Photothermal Stimulus of Femtosecond Pulsed Laser. Advanced Functional Materials, 2014, 24, 4229-4239.	14.9	130
38	Graphdiyne Nanosheet-Based Drug Delivery Platform for Photothermal/Chemotherapy Combination Treatment of Cancer. ACS Applied Materials & amp; Interfaces, 2018, 10, 8436-8442.	8.0	130
39	The synergic regulation of conductivity and Seebeck coefficient in pure polyaniline by chemically changing the ordered degree of molecular chains. Journal of Materials Chemistry A, 2014, 2, 2634-2640.	10.3	126
40	Formation of Mo–Polydopamine Hollow Spheres and Their Conversions to MoO ₂ /C and Mo ₂ C/C for Efficient Electrochemical Energy Storage and Catalyst. Small, 2017, 13, 1701246.	10.0	126
41	Nanosheets assembled layered MoS2/MXene as high performance anode materials for potassium ion batteries. Journal of Power Sources, 2020, 449, 227481.	7.8	125
42	Microstructure and mechanical properties of high performance Mg–Gd based alloys. Materials & Design, 2009, 30, 292-296.	5.1	122
43	Interfacial Model Deciphering Highâ€Voltage Electrolytes for High Energy Density, High Safety, and Fastâ€Charging Lithiumâ€Ion Batteries. Advanced Materials, 2021, 33, e2102964.	21.0	122
44	Multiwall Carbon Nanotubes Mediate Macrophage Activation and Promote Pulmonary Fibrosis Through TGFâ€Î²/Smad Signaling Pathway. Small, 2013, 9, 3799-3811.	10.0	121
45	Large-scale DNS of gas–solid flows on Mole-8.5. Chemical Engineering Science, 2012, 71, 422-430.	3.8	120
46	Morphologically Virusâ€Like Fullerenol Nanoparticles Act as the Dualâ€Functional Nanoadjuvant for HIVâ€1 Vaccine. Advanced Materials, 2013, 25, 5928-5936.	21.0	120
47	Large thermoelectric power factor in polyaniline/graphene nanocomposite films prepared by solution-assistant dispersing method. Journal of Materials Chemistry A, 2014, 2, 11107.	10.3	120
48	Two-dimensional Dirac fermions and quantum magnetoresistance in CaMnBi <mml:math xmlns:mml="http://www.w3.org/1998/Math/MathML" display="inline"><mml:msub><mml:mrow /><mml:mn>2</mml:mn></mml:mrow </mml:msub>. Physical Review B, 2012, 85, .</mml:math 	3.2	114
49	The contributions of metal impurities and tube structure to the toxicity of carbon nanotube materials. NPG Asia Materials, 2012, 4, e32-e32.	7.9	112
50	High aspect ratio γ-MnOOH nanowires for high performance rechargeable nonaqueous lithium–oxygen batteries. Chemical Communications, 2012, 48, 7598.	4.1	109
51	RGO/Co 3 O 4 Composites Prepared Using GO-MOFs as Precursor for Advanced Lithium-ion Batteries and Supercapacitors Electrodes. Electrochimica Acta, 2016, 215, 410-419.	5.2	109
52	Characterization of gold nanorods in vivo by integrated analytical techniques: their uptake, retention, and chemical forms. Analytical and Bioanalytical Chemistry, 2010, 396, 1105-1114.	3.7	108
53	Atmospheric Oxidation Mechanism of Toluene. Journal of Physical Chemistry A, 2014, 118, 4533-4547.	2.5	105
54	Selenium Nanoparticles as an Efficient Nanomedicine for the Therapy of Huntington's Disease. ACS Applied Materials & Interfaces, 2019, 11, 34725-34735.	8.0	101

#	Article	IF	CITATIONS
55	Formation of Highly Oxidized Radicals and Multifunctional Products from the Atmospheric Oxidation of Alkylbenzenes. Environmental Science & Technology, 2017, 51, 8442-8449.	10.0	99
56	Unraveling the New Role of an Ethylene Carbonate Solvation Shell in Rechargeable Metal Ion Batteries. ACS Energy Letters, 2021, 6, 69-78.	17.4	99
57	Metal-Organic Framework Template Synthesis of NiCo ₂ S ₄ @C Encapsulated in Hollow Nitrogen-Doped Carbon Cubes with Enhanced Electrochemical Performance for Lithium Storage. ACS Applied Materials & Interfaces, 2017, 9, 18178-18186.	8.0	98
58	An Empirical Model for the Design of Batteries with High Energy Density. ACS Energy Letters, 2020, 5, 807-816.	17.4	97
59	Polyhydroxylated Metallofullerenols Stimulate ILâ€1β Secretion of Macrophage through TLRs/MyD88/NFâ€₽® Pathway and NLRP ₃ Inflammasome Activation. Small, 2014, 10, 2362-2372.	10.0	96
60	Electrolyteâ€Mediated Stabilization of Highâ€Capacity Microâ€Sized Antimony Anodes for Potassiumâ€lon Batteries. Advanced Materials, 2021, 33, e2005993.	21.0	96
61	Stabilizing effects of atomic Ti doping on high-voltage high-nickel layered oxide cathode for lithium-ion rechargeable batteries. Nano Research, 2022, 15, 4091-4099.	10.4	96
62	Sb nanoparticles encapsulated into porous carbon matrixes for high-performance lithium-ion battery anodes. Journal of Power Sources, 2016, 331, 16-21.	7.8	91
63	Argyrodite Solid Electrolyte with a Stable Interface and Superior Dendrite Suppression Capability Realized by ZnO Co-Doping. ACS Applied Materials & Interfaces, 2019, 11, 40808-40816.	8.0	89
64	Self-assembled large-area Co(OH)2 nanosheets/ionic liquid modified graphene heterostructures toward enhanced energy storage. Journal of Materials Chemistry, 2012, 22, 3404.	6.7	88
65	Model-Based Design of Graphite-Compatible Electrolytes in Potassium-Ion Batteries. ACS Energy Letters, 2020, 5, 2651-2661.	17.4	88
66	SnO ₂ Quantum Dots: Rational Design to Achieve Highly Reversible Conversion Reaction and Stable Capacities for Lithium and Sodium Storage. Small, 2020, 16, e2000681.	10.0	87
67	Immobilized Ferrous Ion and Glucose Oxidase on Graphdiyne and Its Application on One-Step Glucose Detection. ACS Applied Materials & Interfaces, 2019, 11, 2647-2654.	8.0	86
68	Unique Co ₃ O ₄ /nitrogen-doped carbon nanospheres derived from metal–organic framework: insight into their superior lithium storage capabilities and electrochemical features in high-voltage batteries. Journal of Materials Chemistry A, 2018, 6, 12466-12474.	10.3	85
69	Engineered Graphene Oxide Nanocomposite Capable of Preventing the Evolution of Antimicrobial Resistance. ACS Nano, 2019, 13, 11488-11499.	14.6	84
70	Immunological Responses Induced by Blood Protein Coronas on Two-Dimensional MoS ₂ Nanosheets. ACS Nano, 2020, 14, 5529-5542.	14.6	82
71	Evidence of Formation of Bicyclic Species in the Early Stages of Atmospheric Benzene Oxidation. Journal of Physical Chemistry A, 2009, 113, 5385-5396.	2.5	80
72	Inhibitory Effect of Cinnamaldehyde, Citral, and Eugenol on Aflatoxin Biosynthetic Gene Expression and Aflatoxin B ₁ Biosynthesis in <i>Aspergillus flavus</i> . Journal of Food Science, 2015, 80, M2917-24.	3.1	79

#	Article	IF	CITATIONS
73	Synthesis of rhombic hierarchical YF3 nanocrystals and their use as upconversion photocatalysts after TiO2 coating. Nanoscale, 2013, 5, 3030.	5.6	78
74	CuO Nanorod Arrays Formed Directly on Cu Foil from MOFs as Superior Binder-Free Anode Material for Lithium-Ion Batteries. ACS Energy Letters, 2017, 2, 1564-1570.	17.4	78
75	Unraveling Metal Oxide Role in Exfoliating Graphite: New Strategy to Construct Highâ€Performance Grapheneâ€Modified SiO <i>_x</i> â€Based Anode for Lithiumâ€Ion Batteries. Advanced Functional Materials, 2020, 30, 1910657.	14.9	78
76	Engineering Sodium-Ion Solvation Structure to Stabilize Sodium Anodes: Universal Strategy for Fast-Charging and Safer Sodium-Ion Batteries. Nano Letters, 2020, 20, 3247-3254.	9.1	78
77	Selective metabolic effects of gold nanorods on normal and cancer cells and their application in anticancer drug screening. Biomaterials, 2013, 34, 7117-7126.	11.4	77
78	Additives Engineered Nonflammable Electrolyte for Safer Potassium Ion Batteries. Advanced Functional Materials, 2020, 30, 2001934.	14.9	77
79	Tunable Wettability and Rewritable Wettability Gradient from Superhydrophilicity to Superhydrophobicity. Langmuir, 2010, 26, 12203-12208.	3.5	76
80	FeS2@C nanowires derived from organic-inorganic hybrid nanowires for high-rate and long-life lithium-ion batteries. Journal of Power Sources, 2016, 328, 56-64.	7.8	76
81	Facile fabrication of SnO ₂ @TiO ₂ core–shell structures as anode materials for lithium-ion batteries. Journal of Materials Chemistry A, 2016, 4, 12850-12857.	10.3	76
82	Hierarchical Porous Te@ZnCo ₂ O ₄ Nanofibers Derived from Te@Metalâ€Organic Frameworks for Superior Lithium Storage Capability. Advanced Functional Materials, 2017, 27, 1604941.	14.9	76
83	Controllable fabrication of C/Sn and C/SnO/Sn composites as anode materials for high-performance lithium-ion batteries. Chemical Engineering Journal, 2017, 330, 1035-1043.	12.7	76
84	Au@Pt nanostructures: a novel photothermal conversion agent for cancer therapy. Nanoscale, 2014, 6, 3670.	5.6	71
85	Model-Based Design of Stable Electrolytes for Potassium Ion Batteries. ACS Energy Letters, 2020, 5, 3124-3131.	17.4	71
86	Microstructures and tensile properties of Mg–8Gd–0.6Zr–xNd–yY (x+y=3, mass%) alloys. Materials Science & Engineering A: Structural Materials: Properties, Microstructure and Processing, 2006, 433, 133-138.	5.6	70
87	A novel immunochromatographic electrochemical biosensor for highly sensitive and selective detection of trichloropyridinol, a biomarker of exposure to chlorpyrifos. Biosensors and Bioelectronics, 2011, 26, 2835-2840.	10.1	70
88	Core–Shell NiFe ₂ O ₄ @TiO ₂ Nanorods: An Anode Material with Enhanced Electrochemical Performance for Lithiumâ€ion Batteries. Chemistry - A European Journal, 2014, 20, 11214-11219.	3.3	70
89	Gadolinium(III)-Chelated Silica Nanospheres Integrating Chemotherapy and Photothermal Therapy for Cancer Treatment and Magnetic Resonance Imaging. ACS Applied Materials & Interfaces, 2015, 7, 25014-25023.	8.0	70
90	Inhibition of Cancer Cell Migration by Gold Nanorods: Molecular Mechanisms and Implications for Cancer Therapy. Advanced Functional Materials, 2014, 24, 6922-6932.	14.9	69

#	Article	IF	CITATIONS
91	Effect of Y on microstructure and mechanical properties of duplex Mg–7Li alloys. Journal of Alloys and Compounds, 2010, 506, 468-474.	5.5	68
92	Snâ€based Intermetallic Compounds for Liâ€ion Batteries: Structures, Lithiation Mechanism, and Electrochemical Performances. Energy and Environmental Materials, 2018, 1, 132-147.	12.8	68
93	Controlled construction of hierarchical Co _{1â^'x} S structures as high performance anode materials for lithium ion batteries. CrystEngComm, 2014, 16, 814-819.	2.6	66
94	Coated/Sandwiched rGO/CoS _{<i>x</i>} Composites Derived from Metal–Organic Frameworks/GO as Advanced Anode Materials for Lithiumâ€Ion Batteries. Chemistry - A European Journal, 2016, 22, 1467-1474.	3.3	66
95	Largeâ€5cale Fabrication of Core–Shell Structured C/SnO ₂ Hollow Spheres as Anode Materials with Improved Lithium Storage Performance. Small, 2017, 13, 1701993.	10.0	66
96	Emerging Potassiumâ€ion Hybrid Capacitors. ChemSusChem, 2020, 13, 5837-5862.	6.8	65
97	Gd–Metallofullerenol Nanomaterial Suppresses Pancreatic Cancer Metastasis by Inhibiting the Interaction of Histone Deacetylase 1 and Metastasis-Associated Protein 1. ACS Nano, 2015, 9, 6826-6836.	14.6	64
98	Two-step oxidation of bulk Sb to one-dimensional Sb2O4 submicron-tubes as advanced anode materials for lithium-ion and sodium-ion batteries. Chemical Engineering Journal, 2017, 315, 101-107.	12.7	64
99	Highly selective fluorescence turn-on chemosensor based on naphthalimide derivatives for detection of copper(II) ions. Spectrochimica Acta - Part A: Molecular and Biomolecular Spectroscopy, 2013, 105, 57-61.	3.9	63
100	Fabrication of Surfaces with Extremely High Contact Angle Hysteresis from Polyelectrolyte Multilayer. Langmuir, 2011, 27, 15299-15304.	3.5	62
101	A bare-eye-based lateral flow immunoassay based on the use of gold nanoparticles for simultaneous detection of three pesticides. Mikrochimica Acta, 2014, 181, 1565-1572.	5.0	61
102	Silver nanoparticles impede phorbol myristate acetate-induced monocyte–macrophage differentiation and autophagy. Nanoscale, 2015, 7, 16100-16109.	5.6	61
103	Atmospheric oxidation mechanism of naphthalene initiated by OH radical. A theoretical study. Physical Chemistry Chemical Physics, 2012, 14, 2645.	2.8	60
104	General and facile method to fabricate uniform Y2O3:Ln3+ (Ln3+ = Eu3+, Tb3+) hollow microspheres using polystyrene spheres as templates. Journal of Materials Chemistry, 2012, 22, 21695.	6.7	59
105	Inhibitory effects of multiwall carbon nanotubes with high iron impurity on viability and neuronal differentiation in cultured PC12 cells. Toxicology, 2013, 313, 49-58.	4.2	59
106	Electron-hole asymmetry, Dirac fermions, and quantum magnetoresistance in <mml:math xmlns:mml="http://www.w3.org/1998/Math/MathML"><mml:msub><mml:mi>BaMnBi</mml:mi><mml:mn>2Physical Review B, 2016, 93, .</mml:mn></mml:msub></mml:math 	nm&m2n><	/mːɒəː/msub><
107	Stability of Ligands on Nanoparticles Regulating the Integrity of Biological Membranes at the Nano–Lipid Interface. ACS Nano, 2019, 13, 8680-8693.	14.6	59
108	Superhydrophobic SERS substrates based on silver dendrite-decorated filter paper for trace detection	5.4	59

of nitenpyram. Analytica Chimica Acta, 2019, 1049, 170-178.

#	Article	IF	CITATIONS
109	The dose-dependent toxicological effects and potential perturbation on the neurotransmitter secretion in brain following intranasal instillation of copper nanoparticles. Nanotoxicology, 2012, 6, Magnetic states of the two-leg-ladder alkali metal iron selenides <mml:math <="" td="" xmlns:mml="http://www.w3.org/1998/Math/MathML"><td>3.0</td><td>58</td></mml:math>	3.0	58
110	display="inline"> <mml:mi>A</mml:mi> Fe <mml:math xmlns:mml="http://www.w3.org/1998/Math/MathML" display="inline"><mml:msub><mml:mrow /><mml:mn>2</mml:mn></mml:mrow </mml:msub>Se<mml:math xmlns:mml="http://www.w3.org/1998/Math/MathML" display="inline"><mml:msub><mml:mrow< td=""><td>3.2</td><td>58</td></mml:mrow<></mml:msub></mml:math </mml:math 	3.2	58
111	Atmospheric Oxidation Mechanism of <i>m</i> -Xylene Initiated by OH Radical. Journal of Physical Chemistry A, 2014, 118, 10778-10787.	2.5	58
112	Hierarchical N-doped carbon nanosheets submicrospheres enable superior electrochemical properties for potassium ion capacitors. Journal of Power Sources, 2020, 469, 228415.	7.8	57
113	Sodium doping derived electromagnetic center of lithium layered oxide cathode materials with enhanced lithium storage. Nano Energy, 2022, 94, 106900.	16.0	57
114	Detection of Nitrous Acid by Cavity Ring-Down Spectroscopy. Environmental Science & Technology, 2000, 34, 4221-4227.	10.0	56
115	Pulmonary responses to printer toner particles in mice after intratracheal instillation. Toxicology Letters, 2010, 199, 288-300.	0.8	56
116	Chemiluminescence Reaction Kinetics-Resolved Multianalyte Immunoassay Strategy Using a Bispecific Monoclonal Antibody as the Unique Recognition Reagent. Analytical Chemistry, 2015, 87, 2952-2958.	6.5	56
117	Structure and mechanical properties of extruded Mg–Gd based alloy sheet. Materials Science & Engineering A: Structural Materials: Properties, Microstructure and Processing, 2009, 520, 162-167.	5.6	55
118	Direct numerical simulation of particle–fluid systems by combining time-driven hard-sphere model and lattice Boltzmann method. Particuology, 2010, 8, 379-382.	3.6	55
119	Preparation and characterization of MnFe2O4 in the solvothermal process: Their magnetism and electrochemical properties. Materials Research Bulletin, 2013, 48, 2511-2516.	5.2	55
120	Facile synthesis of symmetric bundle-like Sb ₂ S ₃ micron-structures and their application in lithium-ion battery anodes. Chemical Communications, 2016, 52, 7691-7694.	4.1	55
121	Aflatoxin B 1 inhibition in Aspergillus flavus by Aspergillus niger through down-regulating expression of major biosynthetic genes and AFB 1 degradation by atoxigenic A . flavus. International Journal of Food Microbiology, 2017, 256, 1-10.	4.7	54
122	Facile synthesis of CuS/rGO composite with enhanced electrochemical lithium-storage properties through microwave-assisted hydrothermal method. Electrochimica Acta, 2016, 203, 238-245.	5.2	53
123	Fast and Energy Efficient Synthesis of ZnO@RGO and its Application in Ni–Zn Secondary Battery. Journal of Physical Chemistry C, 2016, 120, 12337-12343.	3.1	53
124	Self-Healing Superhydrophobic Materials Showing Quick Damage Recovery and Long-Term Durability. Langmuir, 2017, 33, 9972-9978.	3.5	53
125	Sulfur-Mediated Interface Engineering Enables Fast SnS Nanosheet Anodes for Advanced Lithium/Sodium-Ion Batteries. ACS Applied Materials & Interfaces, 2020, 12, 25786-25797.	8.0	53
126	Short Multiwall Carbon Nanotubes Promote Neuronal Differentiation of PC12 Cells via Upâ€Regulation of the Neurotrophin Signaling Pathway. Small, 2013, 9, 1786-1798.	10.0	52

#	Article	IF	CITATIONS
127	Enhanced electrochemical performances of FeO _x –graphene nanocomposites as anode materials for alkaline nickel–iron batteries. RSC Advances, 2014, 4, 15394-15399.	3.6	52
128	Freestanding MnO2@carbon papers air electrodes for rechargeable Li-O2 batteries. Journal of Power Sources, 2014, 261, 311-316.	7.8	52
129	New Mechanism for the Atmospheric Oxidation of Dimethyl Sulfide. The Importance of Intramolecular Hydrogen Shift in a CH ₃ SCH ₂ OO Radical. Journal of Physical Chemistry A, 2015, 119, 112-117.	2.5	52
130	Unravel the Catalytic Effect of Two-Dimensional Metal Sulfides on Polysulfide Conversions for Lithium–Sulfur Batteries. ACS Applied Materials & Interfaces, 2020, 12, 43560-43567.	8.0	52
131	Solvothermal synthesis of GO/V ₂ O ₅ composites as a cathode material for rechargeable magnesium batteries. RSC Advances, 2015, 5, 76352-76355.	3.6	51
132	Facile synthesis of one-dimensional hollow Sb2O3@TiO2 composites as anode materials for lithium ion batteries. Journal of Power Sources, 2018, 389, 214-221.	7.8	51
133	Elucidating the Nature of the Cu(I) Active Site in CuO/TiO ₂ for Excellent Low-Temperature CO Oxidation. ACS Applied Materials & Interfaces, 2020, 12, 7091-7101.	8.0	51
134	Effects of cerium on the microstructure and mechanical properties of Mg–20Zn–8Al alloy. Materials Science & Engineering A: Structural Materials: Properties, Microstructure and Processing, 2008, 474, 317-322.	5.6	50
135	Mapping of Daily Mean Air Temperature in Agricultural Regions Using Daytime and Nighttime Land Surface Temperatures Derived from TERRA and AQUA MODIS Data. Remote Sensing, 2015, 7, 8728-8756.	4.0	50
136	Understanding Ostwald Ripening and Surface Charging Effects in Solvothermallyâ€Prepared Metal Oxide–Carbon Anodes for High Performance Rechargeable Batteries. Advanced Energy Materials, 2019, 9, 1902194.	19.5	50
137	Microstructures and mechanical properties of as-cast Mg–5Al–0.4Mn–xNd (x=0, 1, 2 and 4) alloys. Materials Science & Engineering A: Structural Materials: Properties, Microstructure and Processing, 2008, 472, 332-337.	5.6	49
138	Effects of Sn content on the microstructure and mechanical properties of Mg–7Zn–5Al based alloys. Materials Science & Engineering A: Structural Materials: Properties, Microstructure and Processing, 2010, 527, 7002-7007.	5.6	49
139	Microstructure, texture and mechanical properties of a hot rolled Mg–6.5Gd–1.3Nd–0.7Y–0.3Zn alloy. Materials & Design, 2012, 34, 776-781.	5.1	49
140	One-pot chemical route for morphology-controllable fabrication of Sn-Sb micro/nano-structures: Advanced anode materials for lithium and sodium storage. Journal of Power Sources, 2017, 342, 861-871.	7.8	49
141	Electron Compensation Effect Suppressed Silver Ion Release and Contributed Safety of Au@Ag Core–Shell Nanoparticles. Nano Letters, 2019, 19, 4478-4489.	9.1	49
142	Electrochemical corrosion behavior of Mg–5Al–0.4Mn–xNd in NaCl solution. Corrosion Science, 2009, 51, 1328-1333.	6.6	48
143	Atmospheric Oxidation Mechanism of Benzene. Fates of Alkoxy Radical Intermediates and Revised Mechanism. Journal of Physical Chemistry A, 2013, 117, 14163-14168.	2.5	47
144	Microstructures and mechanical properties of the Mg–4.5Zn–xGd (x=0, 2, 3 and 5) alloys. Journal of Alloys and Compounds, 2008, 459, 274-280.	5.5	46

#	Article	IF	CITATIONS
145	Integrated analytical techniques with high sensitivity for studying brain translocation and potential impairment induced by intranasally instilled copper nanoparticles. Toxicology Letters, 2014, 226, 70-80.	0.8	46
146	Polyhydroxylated fullerenols regulate macrophage for cancer adoptive immunotherapy and greatly inhibit the tumor metastasis. Nanomedicine: Nanotechnology, Biology, and Medicine, 2016, 12, 945-954.	3.3	46
147	Microstructure and mechanical property of Mg–8.31Gd–1.12Dy–0.38Zr alloy. Materials Science & Engineering A: Structural Materials: Properties, Microstructure and Processing, 2008, 477, 193-197.	5.6	45
148	Yolk@Shell or Concave Cubic NiO–Co ₃ O ₄ @C Nanocomposites Derived from Metal–Organic Frameworks for Advanced Lithium-Ion Battery Anodes. Inorganic Chemistry, 2017, 56, 9794-9801.	4.0	45
149	Mechanistic Studies of the Pyrolysis of 1,3-Butadiene, 1,3-Butadiene-1,1,4,4-d4, 1,2-Butadiene, and 2-Butyne by Supersonic Jet/Photoionization Mass Spectrometry. Journal of Physical Chemistry A, 2005, 109, 2190-2196.	2.5	44
150	Tunable wettability by counterion exchange at the surface of electrostatic self-assembled multilayers. Chemical Communications, 2008, , 5972.	4.1	44
151	Preparation and luminescence of La ₂ O ₃ :Ln ³⁺ (Ln ³⁺ =) Tj ET	Qq1 1 0.78 3.6	84314 rgBT /(44
152	Lattice Boltzmann based discrete simulation for gas–solid fluidization. Chemical Engineering Science, 2013, 101, 228-239.	3.8	44
153	A bare-eye based one-step signal amplified semiquantitative immunochromatographic assay for the detection of imidacloprid in Chinese cabbage samples. Analytica Chimica Acta, 2015, 881, 82-89.	5.4	44
154	Constructing Dense SiO _{<i>x</i>} @Carbon Nanotubes versus Spinel Cathode for Advanced Highâ€Energy Lithiumâ€Ion Batteries. ChemElectroChem, 2017, 4, 1165-1171.	3.4	44
155	Electrochemical hydrogen storage in (Ti1â~V)2Ni (x= 0.05–0.3) alloys comprising icosahedral quasicrystalline phase. Electrochimica Acta, 2009, 54, 2770-2773.	5.2	43
156	Enzyme-linked immunosorbent assay for detection of organophosphorylated butyrylcholinesterase: A biomarker of exposure to organophosphate agents. Analytica Chimica Acta, 2011, 693, 1-6.	5.4	43
157	A new colorimetric and fluorescent bifunctional probe for Cu2+ and Fâ^' ions based on perylene bisimide derivatives. Tetrahedron Letters, 2014, 55, 3218-3222.	1.4	43
158	Liquid Marbles Supported by Monodisperse Poly(methylsilsesquioxane) Particles. Langmuir, 2014, 30, 9071-9075.	3.5	43
159	Improvement in ion transport in Na3PSe4–Na3SbSe4 by Sb substitution. Journal of Materials Science, 2018, 53, 1987-1994.	3.7	43
160	Catalysis of silica-based anode (de-)lithiation: compositional design within a hollow structure for accelerated conversion reaction kinetics. Journal of Materials Chemistry A, 2020, 8, 12306-12313.	10.3	43
161	Counterion exchange at the surface of polyelectrolyte multilayer film for wettability modulation. Soft Matter, 2009, 5, 2072.	2.7	42
162	The atmospheric oxidation mechanism of 1,2,4-trimethylbenzene initiated by OH radicals. Physical Chemistry Chemical Physics, 2014, 16, 17908.	2.8	42

#	Article	IF	CITATIONS
163	Microstructures and mechanical properties of Mg–8Gd–0.6Zr–xNd (xÂ=Â0, 1, 2 and 3 mass%) alloys. Journal of Materials Science, 2007, 42, 3908-3913.	3.7	41
164	Simple and Improved Approaches to Long-Lasting, Hydrophilic Silicones Derived from Commercially Available Precursors. ACS Applied Materials & Interfaces, 2014, 6, 22876-22883.	8.0	41
165	Electrochemical activation, voltage decay and hysteresis of Li-rich layered cathode probed by various cobalt content. Electrochimica Acta, 2018, 265, 115-120.	5.2	41
166	Cooperative effect of Co and Al on the microstructure and electrochemical properties of AB3-type hydrogen storage electrode alloys for advanced MH/Ni secondary battery. International Journal of Hydrogen Energy, 2011, 36, 893-900.	7.1	40
167	Atmospheric Oxidation Mechanism of Phenol Initiated by OH Radical. Journal of Physical Chemistry A, 2013, 117, 2358-2364.	2.5	40
168	Sustainable solid-state strategy to hierarchical core-shell structured Fe3O4@graphene towards a safer and green sodium ion full battery. Electrochimica Acta, 2018, 260, 882-889.	5.2	40
169	Morphology Evolution and Control of Moâ€polydopamine Coordination Complex from 2D Single Nanopetal to Hierarchical Microflowers. Small, 2018, 14, e1800090.	10.0	40
170	Kinetic and electrochemical properties of icosahedral quasicrystalline Ti45Zr35Ni17Cu3Ti45Zr35Ni17Cu3 powder. International Journal of Hydrogen Energy, 2006, 31, 1394-1400.	7.1	39
171	The influence of mischmetal and tin on the microstructure and mechanical properties of Mg–6Zn–5Al-based alloys. Acta Materialia, 2008, 56, 934-941.	7.9	39
172	Microstructure and mechanical properties of Mg–4.5Zn–xNd (x=0, 1 and 2, wt%) alloys. Materials Science & Engineering A: Structural Materials: Properties, Microstructure and Processing, 2008, 479, 339-344.	5.6	39
173	A Core–Shell Fe/Fe ₂ O ₃ Nanowire as a Highâ€Performance Anode Material for Lithiumâ€lon Batteries. Chemistry - A European Journal, 2016, 22, 12081-12087.	3.3	39
174	One-step synthesis of Ni3Sn2@reduced graphene oxide composite with enhanced electrochemical lithium storage properties. Electrochimica Acta, 2016, 192, 188-195.	5.2	39
175	Preparation of bamboo carbon fiber and sandwich-like bamboo carbon fiber@SnO2@carbon composites and their potential application in structural lithium-ion battery anodes. Journal of Alloys and Compounds, 2017, 709, 227-233.	5.5	39
176	A highly promising high-nickel low-cobalt lithium layered oxide cathode material for high-performance lithium-ion batteries. Journal of Colloid and Interface Science, 2021, 597, 334-344.	9.4	39
177	Ab initio study of reaction of dimethyl sulfoxide (DMSO) with OH radical. Chemical Physics Letters, 2002, 356, 490-496.	2.6	38
178	Twinning and dynamic precipitation upon hot compression of a Mgâ^'Gdâ^'Yâ^'Ndâ^'Zr alloy. Journal of Alloys and Compounds, 2012, 525, 103-109.	5.5	38
179	Effect of Cinnamaldehyde on Morphological Alterations of Aspergillus ochraceus and Expression of Key Genes Involved in Ochratoxin A Biosynthesis. Toxins, 2018, 10, 340.	3.4	38
180	A microchip-based model wound with multiple types of cells. Lab on A Chip, 2011, 11, 2819.	6.0	37

181	Synthesis and performance of polyurethane coated urea as slow/controlled release fertilizer. Journal Wuhan University of Technology, Materials Science Edition, 2012, 27, 126-129.	1.0	37
182	SnO ₂ nanocrystals anchored on N-doped graphene for high-performance lithium storage. Chemical Communications, 2015, 51, 3660-3662.	4.1	37
183	Comparative Proteomics Reveals that Phosphorylation of β Carbonic Anhydrase 1 Might be Important for Adaptation to Drought Stress in Brassica napus. Scientific Reports, 2016, 6, 39024.	3.3	37
184	The effect of La or Ce on ageing response and mechanical properties of cast Mg–Gd–Zr alloys. Materials Characterization, 2008, 59, 435-439.	4.4	36
185	Investigations of the properties of Mg–5Al–0.3Mn–xCe (x=0–3, wt.%) alloys. Journal of Alloys and Compounds, 2009, 477, 341-345.	5.5	36
186	A novel strategy to prepare Sb thin film sandwiched between the reduced graphene oxide and Ni foam as binder-free anode material for lithium-ion batteries. Electrochimica Acta, 2016, 190, 804-810.	5.2	36
187	Selfâ€Assembly of Hierarchical Niâ€Moâ€Polydopamine Microflowers and their Conversion to a Niâ€Mo ₂ C/C Composite for Water Splitting. Chemistry - A European Journal, 2017, 23, 4644-4650.	3.3	36
188	A Kind of Coordination Complex Cement for the Self-Assembly of Superstructure. ACS Nano, 2018, 12, 4002-4009.	14.6	36
189	Response of Surface Temperature to Afforestation in the Kubuqi Desert, Inner Mongolia. Journal of Geophysical Research D: Atmospheres, 2018, 123, 948-964.	3.3	36
190	Formation of porous ZnO microspheres and its application as anode material with superior cycle stability in zinc-nickel secondary batteries. Journal of Power Sources, 2018, 396, 615-620.	7.8	36
191	Electrochemical properties of amorphous and icosahedral quasicrystalline Ti45Zr35Ni17Cu3 powders. Journal of Power Sources, 2006, 159, 1458-1463.	7.8	35
192	In vivo pharmacokinetic features and biodistribution of star and rod shaped gold nanoparticles by multispectral optoacoustic tomography. RSC Advances, 2015, 5, 7529-7538.	3.6	35
193	Synthesis and performances of carbon fiber@Co3O4 based on metal organic frameworks as anode materials for structural lithium-ion battery. Journal of Electroanalytical Chemistry, 2017, 807, 196-202.	3.8	35
194	Insight of Enhanced Redox Chemistry for Porous MoO ₂ Carbon-Derived Framework as Polysulfide Reservoir in Lithium–Sulfur Batteries. ACS Applied Materials & Interfaces, 2018, 10, 42286-42293.	8.0	35
195	Structure stability and strengthening mechanism of die-cast Mg–Gd–Dy based alloy. Journal of Alloys and Compounds, 2009, 469, 587-592.	5.5	34
196	Effect of hot rolling on the microstructure and mechanical properties of Mg–5Al–0.3Mn–2Nd alloy. Journal of Alloys and Compounds, 2010, 507, 178-183.	5.5	34
197	Effects of Metal Ions and Ligand Functionalization on Hydrogen Storage in Metal–Organic Frameworks by Spillover. Journal of Physical Chemistry C, 2011, 115, 13829-13836.	3.1	34
198	A Facile Moltenâ€Salt Route for Largeâ€Scale Synthesis of NiFe 2 O 4 Nanoplates with Enhanced Lithium Storage Capability. Chemistry - A European Journal, 2015, 21, 14140-14145.	3.3	34

#	Article	IF	CITATIONS
199	Insight into the Coprecipitation-Controlled Crystallization Reaction for Preparing Lithium-Layered Oxide Cathodes. ACS Applied Materials & Interfaces, 2021, 13, 717-726.	8.0	34
200	All-Starch-Based Hydrogel for Flexible Electronics: Strain-Sensitive Batteries and Self-Powered Sensors. ACS Sustainable Chemistry and Engineering, 2022, 10, 6724-6735.	6.7	34
201	Synthesis and electrochemical properties of LiFePO4/C composite cathode material prepared by a new route using supercritical carbon dioxide as a solvent. Journal of Materials Chemistry, 2011, 21, 6975.	6.7	33
202	Novel ε-Cu0.95V2O5 hollow microspheres and α-CuV2O6 nanograins: Facile synthesis and application in lithium-ion batteries. Journal of Power Sources, 2013, 237, 112-118.	7.8	33
203	Dual Doping: An Effective Method to Enhance the Electrochemical Properties of Li ₁₀ GeP ₂ S ₁₂ â€Based Solid Electrolytes. Journal of the American Ceramic Society, 2015, 98, 3831-3835.	3.8	33
204	Identification and Characterization of a Glyoxalase I Gene in a Rapeseed Cultivar with Seed Thermotolerance. Frontiers in Plant Science, 2016, 7, 150.	3.6	33
205	Variation in fungal microbiome (mycobiome) and aflatoxins during simulated storage of in-shell peanuts and peanut kernels. Scientific Reports, 2016, 6, 25930.	3.3	33
206	Metabolic Characteristics of 16HBE and A549 Cells Exposed to Different Surface Modified Gold Nanorods. Advanced Healthcare Materials, 2016, 5, 2363-2375.	7.6	33
207	Atmospheric Oxidation of Furan and Methyl-Substituted Furans Initiated by Hydroxyl Radicals. Journal of Physical Chemistry A, 2017, 121, 9306-9319.	2.5	33
208	A simplified two-fluid model coupled with EMMS drag for gas-solid flows. Powder Technology, 2017, 314, 299-314.	4.2	33
209	High alkaline ion storage capacity of hollow interwoven structured Sb/TiO ₂ particles: the galvanic replacement formation mechanism and volumetric buffer effect. Chemical Communications, 2018, 54, 4049-4052.	4.1	33
210	Primary Formation of Highly Oxidized Multifunctional Products in the OH-Initiated Oxidation of Isoprene: A Combined Theoretical and Experimental Study. Environmental Science & Technology, 2018, 52, 12255-12264.	10.0	33
211	Metal organic frameworks route to prepare two-dimensional porous zinc-cobalt oxide plates as anode materials for lithium-ion batteries. Journal of Power Sources, 2018, 396, 659-666.	7.8	33
212	Development of an Enzyme Linked Immunosorbent Assay and an Immunochromatographic Assay for Detection of Organophosphorus Pesticides in Different Agricultural Products. PLoS ONE, 2012, 7, e53099.	2.5	33
213	Addition complexes of dimethyl sulfide (DMS) and OH radical and their reactions with O 2 by ab initio and density functional theory. Computational and Theoretical Chemistry, 2001, 543, 167-175.	1.5	32
214	A retrievable and highly selective fluorescent probe for monitoring dihydrogen phosphate ions based on a naphthalimide framework. Spectrochimica Acta - Part A: Molecular and Biomolecular Spectroscopy, 2013, 114, 323-329.	3.9	32
215	A method of two-stage clustering learning based on improved DBSCAN and density peak algorithm. Computer Communications, 2021, 167, 75-84.	5.1	32
216	Microstructure and mechanical properties of extruded Mg–8Gd–2Y–1Nd–0.3Zn–0.6Zr alloy. Materials Science & Engineering A: Structural Materials: Properties, Microstructure and Processing, 2011, 528, 7805-7810.	5.6	31

#	Article	IF	CITATIONS
217	Electrochemical hydrogen storage properties of Ti1.4V0.6Ni alloy comprising quasicrystal coating with Cu. Journal of Alloys and Compounds, 2015, 650, 15-21.	5.5	31
218	Ammonia-low coprecipitation synthesis of lithium layered oxide cathode material for high-performance battery. Chemical Engineering Journal, 2021, 411, 128487.	12.7	31
219	Formations of amorphous and quasicrystal phases in Ti–Zr–Ni–Cu alloys. Journal of Alloys and Compounds, 2003, 361, 234-240.	5.5	30
220	Clusters of Hydrated Methane Sulfonic Acid CH3SO3H·(H2O)n(n= 1â^'5): A Theoretical Study. Journal of Physical Chemistry A, 2007, 111, 3642-3651.	2.5	30
221	Influences of Gd on the microstructure and strength of Mg–4.5Zn alloy. Materials Characterization, 2008, 59, 1667-1674.	4.4	30
222	Age hardening and mechanical properties of Mg–Gd–Er alloy. Journal of Alloys and Compounds, 2008, 456, 395-399.	5.5	30
223	Cinnabar is not converted into methylmercury by human intestinal bacteria. Journal of Ethnopharmacology, 2011, 135, 110-115.	4.1	30
224	Large magnetothermopower effect in Dirac materials (Sr/Ca)MnBi ₂ . Applied Physics Letters, 2012, 100, 112111.	3.3	30
225	Multi-analyte enzyme-linked immunosorbent assay for organophosphorus pesticides and neonicotinoid insecticides using a bispecific monoclonal antibody. Analytical Methods, 2013, 5, 1556.	2.7	30
226	Synthesis, Structure, Electronic State, and Luminescent Properties of Novel Blueâ€Lightâ€Emitting Arylâ€Substituted 9,9â€Di(4â€(diâ€ <i>p</i> â€tolyl)aminophenyl)fluorenes. Advanced Functional Materials, 2008 18, 2335-2347.	3, 14.9	29
227	Microstructures and mechanical properties of as-cast Mg–5Y–3Nd–Zr–xGd (x=0, 2 and 4wt.%) alloys. Materials Science & Engineering A: Structural Materials: Properties, Microstructure and Processing, 2010, 527, 1891-1895.	5.6	29
228	A cerium–lead redox flow battery system employing supporting electrolyte of methanesulfonic acid. Journal of Power Sources, 2015, 295, 28-32.	7.8	29
229	Synthesis of Porous NiO Nanorods as Highâ€Performance Anode Materials for Lithiumâ€lon Batteries. Particle and Particle Systems Characterization, 2016, 33, 764-770.	2.3	29
230	Ultrathin SnO2 nanosheets anchored on graphene with improved electrochemical kinetics for reversible lithium and sodium storage. Applied Surface Science, 2019, 484, 646-654.	6.1	29
231	The influences of rare earth content on the microstructure and mechanical properties of Mg–7Zn–5Al alloy. Materials & Design, 2010, 31, 3542-3549.	5.1	28
232	Electrochemical performance of TiVNi-Quasicrystal and AB3-Type hydrogen storage alloy composite materials. International Journal of Hydrogen Energy, 2011, 36, 616-620.	7.1	28
233	Fe–salphen complexes from intracellular pH-triggered degradation ofÂFe3O4@Salphen-InIII CPPs for selectively killing cancer cells. Biomaterials, 2014, 35, 1676-1685.	11.4	28
234	Ferroxidase-like activity of Au nanorod/Pt nanodot structures and implications for cellular oxidative stress. Nano Research, 2015, 8, 4024-4037.	10.4	28

#	Article	IF	CITATIONS
235	SERS Assay for Copper(II) Ions Based on Dual Hot-Spot Model Coupling with MarR Protein: New Cu ²⁺ -Specific Biorecognition Element. Analytical Chemistry, 2017, 89, 6392-6398.	6.5	28
236	Entropic elasticity and negative thermal expansion in a simple cubic crystal. Science Advances, 2019, 5, eaay2748.	10.3	28
237	Immobilization of mercury by nano-elemental selenium and the underlying mechanisms in hydroponic-cultured garlic plant. Environmental Science: Nano, 2020, 7, 1115-1125.	4.3	28
238	Anti-catalytic and zincophilic layers integrated zinc anode towards efficient aqueous batteries for ultra-long cycling stability. Nano Research, 2022, 15, 8076-8082.	10.4	28
239	Ab initio calculation on thermochemistry of CH3SOxH (x=1–3) and H2SOy (y=2,3). Computational and Theoretical Chemistry, 2002, 581, 129-138.	1.5	27
240	The microstructures and mechanical properties of cast Mg–Zn–Al–RE alloys. Journal of Alloys and Compounds, 2009, 480, L33-L36.	5.5	27
241	Atmospheric Oxidation Mechanism of Furfural Initiated by Hydroxyl Radicals. Journal of Physical Chemistry A, 2017, 121, 3247-3253.	2.5	27
242	Carbon fiber@ pore-ZnO composite as anode materials for structural lithium-ion batteries. Journal of Electroanalytical Chemistry, 2019, 833, 39-46.	3.8	27
243	Facile Preparation of Eco-Friendly, Flexible Starch-Based Materials with Ionic Conductivity and Strain-Responsiveness. ACS Sustainable Chemistry and Engineering, 2020, 8, 19117-19128.	6.7	27
244	Cavity Ring-Down Spectroscopy of Ambient NO2with Quantification and Elimination of Interferences. Environmental Science & Technology, 2006, 40, 7868-7873.	10.0	26
245	Electrochemical corrosion behavior of cast Mg–Al–RE–Mn Alloys in NaCl solution. Journal of Materials Science, 2008, 43, 2550-2554.	3.7	26
246	A novel method to prepare Ti1.4V0.6Ni alloy covered with carbon and nanostructured Co3O4, and its good electrochemical hydrogen storage properties as negative electrode material for Ni-MH battery. Electrochimica Acta, 2016, 222, 1716-1723.	5.2	26
247	A rational design to buffer volume expansion of CoSn intermetallic in lithium and sodium storage: Multicore-shell versus monocore-shell. Energy Storage Materials, 2019, 23, 629-635.	18.0	26
248	Structural Disorganization and Chain Aggregation of High-Amylose Starch in Different Chloride Salt Solutions. ACS Sustainable Chemistry and Engineering, 2020, 8, 4838-4847.	6.7	26
249	An SiO _x anode strengthened by the self-catalytic growth of carbon nanotubes. Nanoscale, 2021, 13, 3808-3816.	5.6	26
250	Gospel for Improving the Lithium Storage Performance of High-Voltage High-Nickel Low-Cobalt Layered Oxide Cathode Materials. ACS Applied Materials & Interfaces, 2021, 13, 58871-58884.	8.0	26
251	Microstructure, texture and mechanical properties of extruded Mg–5Al–2Nd–0.2Mn alloy. Journal of Alloys and Compounds, 2015, 653, 100-107.	5.5	25
252	Enhanced cycling performance of Se-doped SnS carbon nanofibers as negative electrode for lithium-ion batteries. Journal of Alloys and Compounds, 2017, 695, 1294-1300.	5.5	25

#	Article	IF	CITATIONS
253	Enabling high electrochemical activity of a hollow SiO ₂ anode by decorating it with ultrafine cobalt nanoparticles and a carbon matrix for long-lifespan lithium ion batteries. Nanoscale, 2020, 12, 13442-13449.	5.6	25
254	Determinants of the Asymmetric Parameter in the Generalized Complementary Principle of Evaporation. Water Resources Research, 2020, 56, e2019WR026570.	4.2	25
255	Microstructure and electrochemical hydrogen storage characteristics of (La0.7Mg0.3)1â^Ce Ni2.8Co0.5 (x= 0–0.20) electrode alloys. International Journal of Hydrogen Energy, 2011, 36, 3016-3021.	7.1	24
256	Development of a Specific Enzyme-Linked Immunosorbent Assay (ELISA) for the Analysis of the Organophosphorous Pesticide Fenthion in Real Samples Based on Monoclonal Antibody. Analytical Letters, 2011, 44, 1591-1601.	1.8	24
257	Self-assembled growth of LuVO4 nanoleaves: hydrothermal synthesis, morphology evolution, and luminescence properties. RSC Advances, 2012, 2, 11067.	3.6	24
258	Hydrothermal synthesis and characterization of MnCo2O4 in the low-temperature hydrothermal process: Their magnetism and electrochemical properties. Journal of Advanced Ceramics, 2013, 2, 266-273.	17.4	24
259	The atmospheric oxidation of dimethyl, diethyl, and diisopropyl ethers. The role of the intramolecular hydrogen shift in peroxy radicals. Physical Chemistry Chemical Physics, 2016, 18, 7707-7714.	2.8	24
260	PAN-based carbon fiber@SnO2 for highly reversible structural lithium-ion battery anode. Ionics, 2018, 24, 1049-1055.	2.4	24
261	Nanosized FexNi2-xP embedded phosphorus-doped carbon nanorods with superior lithium storage performance. Energy Storage Materials, 2018, 12, 103-109.	18.0	24
262	Spherical hybrid hierarchical porous structure: A plastic model with tunable inner pores for lithium-sulfur batteries. Carbon, 2019, 153, 691-698.	10.3	24
263	Lithium dendrite-free plating/stripping: a new synergistic lithium ion solvation structure effect for reliable lithium–sulfur full batteries. Chemical Communications, 2019, 55, 5713-5716.	4.1	24
264	Single-Particle Analysis for Structure and Iron Chemistry of Atmospheric Particulate Matter. Analytical Chemistry, 2020, 92, 975-982.	6.5	24
265	Bio-inspired heteroatom-doped hollow aurilave-like structured carbon for high-performance sodium-ion batteries and supercapacitors. Journal of Power Sources, 2020, 461, 228128.	7.8	24
266	Highly Unsaturated Hydrogenated Silicon Clusters, SinHx(n= 3â^'10,x= 0â^'3), in Flash Pyrolysis of Silane and Disilane. Journal of Physical Chemistry A, 2002, 106, 5081-5087.	2.5	23
267	Crystallographic and electrochemical characteristics of Ti–Zr–Ni–Pd quasicrystalline alloys. International Journal of Hydrogen Energy, 2009, 34, 6925-6929.	7.1	23
268	Effects of Disordered Ru Substitution inBaFe2As2: Possible Realization of Superdiffusion in Real Materials. Physical Review Letters, 2013, 110, 037001.	7.8	23
269	Mesoporous MFe2O4 (M=Mn, Co, and Ni) for anode materials of lithium-ion batteries: Synthesis and electrochemical properties. Materials Research Bulletin, 2015, 61, 195-200.	5.2	23
270	Highly uniform Co9S8 nanoparticles grown on graphene nanosheets as advanced anode materials for improved Li-storage performance. Applied Surface Science, 2016, 390, 86-91.	6.1	23

#	Article	IF	CITATIONS
271	Double-network hydrogels with superior self-healing properties using starch reinforcing strategy. Carbohydrate Polymers, 2021, 257, 117626.	10.2	23
272	Excellent catalytic effect of LaNi5 on hydrogen storage properties for aluminium hydride at mild temperature. International Journal of Hydrogen Energy, 2021, 46, 38733-38740.	7.1	23
273	Formation of Ti-Zr(Hf)-Ni-Cu Amorphous Alloys and Quasicrystal Precipitation upon Annealing. Materials Transactions, 2001, 42, 528-531.	1.2	22
274	Theoretical Study on the Thermochemistry of Chlorinated and Fluorinated Germanes and Their Radical Fragments. Journal of Physical Chemistry A, 2004, 108, 10346-10353.	2.5	22
275	On the origin of the Murchison meteorite phosphonates. Implications for pre-biotic chemistry. Chemical Communications, 2006, , 1643.	4.1	22
276	Hydrogen absorption in Ti45Zr35Ni17Cu3Ti45Zr35Ni17Cu3 amorphous and quasicrystalline alloy powders. International Journal of Hydrogen Energy, 2007, 32, 2429-2433.	7.1	22
277	Microstructure and Elevated Temperature Properties of Die-cast AZ91-xNd Magnesium Alloys. Journal of Materials Engineering and Performance, 2008, 17, 725-729.	2.5	22
278	Investigation on the microstructure and mechanical properties of a cast Mg–6Zn–5Al–4RE alloy. Journal of Alloys and Compounds, 2008, 458, 178-183.	5.5	22
279	Effects of samarium on microstructures and tensile properties of Mg–5Al–0.3Mn alloy. Materials Science & Engineering A: Structural Materials: Properties, Microstructure and Processing, 2011, 528, 4115-4119.	5.6	22
280	Hydrophobization of Inorganic Oxide Surfaces Using Dimethylsilanediol. Langmuir, 2013, 29, 1329-1332.	3.5	22
281	Atmospheric oxidation mechanism of chlorobenzene. Chemosphere, 2014, 111, 537-544.	8.2	22
282	Overexpression of maize sucrose non-fermenting-1-related protein kinase 1 genes, ZmSnRK1s, causes alteration in carbon metabolism and leaf senescence in Arabidopsis thaliana. Gene, 2019, 691, 34-44.	2.2	22
283	A Designed Durable Electrolyte for Highâ€Voltage Lithiumâ€Ion Batteries and Mechanism Analysis. Chemistry - A European Journal, 2020, 26, 7930-7936.	3.3	22
284	Crystallographic and electrochemical characteristics of icosahedral quasicrysyalline Ti45â^'xZr35â^'xNi17+2xCu3 (x=0–8) powders. Journal of Power Sources, 2006, 162, 713-718.	7.8	21
285	Halogenated silanes, radicals, and cations: Theoretical predictions on ionization energies, structures and potential energy surfaces of cations, proton affinities, and enthalpies of formation. International Journal of Mass Spectrometry, 2008, 276, 56-76.	1.5	21
286	Aging behavior and mechanical properties of Mg–Gd–Ho alloys. Materials Characterization, 2008, 59, 983-986.	4.4	21
287	Nanostructured Carbon/Antimony Composites as Anode Materials for Lithiumâ€lon Batteries with Long Life. Chemistry - an Asian Journal, 2016, 11, 2173-2180.	3.3	21
288	Fabrication of One-Dimensional Sb@TiO ₂ Composites as Anode Materials for Lithium-Ion Batteries. Journal of the Electrochemical Society, 2016, 163, A2641-A2646.	2.9	21

#	Article	IF	CITATIONS
289	High electrochemical performance of nanoporous Fe3O4/CuO/Cu composites synthesized by dealloying Al-Cu-Fe quasicrystal. Journal of Alloys and Compounds, 2017, 729, 360-369.	5.5	21
290	Mechanism of Gas-Phase Ozonolysis of Î ² -Myrcene in the Atmosphere. Journal of Physical Chemistry A, 2018, 122, 3013-3020.	2.5	21
291	Advanced and safer lithium-ion battery based on sustainable electrodes. Journal of Power Sources, 2018, 379, 53-59.	7.8	21
292	Microwave-assisted synthesis of the sandwich-like porous Al2O3/RGO nanosheets anchoring NiO nanocomposite as anode materials for lithium-ion batteries. Applied Surface Science, 2018, 427, 354-362.	6.1	21
293	Multifunctional sulfur-mediated strategy enabling fast-charging Sb ₂ S ₃ micro-package anode for lithium-ion storage. Journal of Materials Chemistry A, 2021, 9, 7838-7847.	10.3	21
294	Atmospheric oxidation mechanisms of polychlorinated dibenzo-p-dioxins are different from those of benzene and dibenzofuran: A theoretical prediction. Chemosphere, 2011, 82, 782-785.	8.2	20
295	Atmospheric Oxidation Mechanism of 2,7-Dimethylnaphthalene is Different from That of Monocyclic Aromatic Benzenes. A Theoretical Study. Journal of Physical Chemistry A, 2013, 117, 160-168.	2.5	20
296	Intensive suppression of thermal conductivity in Nd0.6Fe2Co2Sb12-xGex through spontaneous precipitates. Journal of Applied Physics, 2013, 114, 083715.	2.5	20
297	Structure Design and Performance of LiNi _x Co _y Mn _{1â€xâ€y} O ₂ Cathode Materials for Lithiumâ€ion Batteries: A Review. Journal of the Chinese Chemical Society, 2014, 61, 1071-1083.	1.4	20
298	Tin dioxide as a high-performance catalyst towards Ce(<scp>vi</scp>)/Ce(<scp>iii</scp>) redox reactions for redox flow battery applications. Journal of Materials Chemistry A, 2017, 5, 5036-5043.	10.3	20
299	Enhanced electrochemical hydrogen storage performance of Ti V Ni composite employing NaAlH 4. International Journal of Hydrogen Energy, 2017, 42, 14633-14640.	7.1	20
300	Hierarchical porous CoNi/CoO/NiO composites derived from dealloyed quasicrystals as advanced anodes for lithium-ion batteries. Scripta Materialia, 2017, 139, 30-33.	5.2	20
301	Bioinspired Architectures and Heteroatom Doping To Construct Metalâ€Oxideâ€Based Anode for Highâ€Performance Lithiumâ€Ion Batteries. Chemistry - A European Journal, 2018, 24, 16902-16909.	3.3	20
302	Surface-functionalized graphite felts: Enhanced performance in cerium-based redox flow batteries. Carbon, 2018, 138, 363-368.	10.3	20
303	Mesoporous yolk-shell ZnO/C microspheres as active ingredient of zinc anode with outstanding cycle stability and high rate performance. Journal of Alloys and Compounds, 2019, 795, 391-400.	5.5	20
304	Structure and electrochemical characteristics of melted composite Ti0.10Zr0.15V0.35Cr0.10Ni0.30–LaNi5 hydrogen storage alloys. Electrochimica Acta, 2008, 53, 7831-7837.	5.2	19
305	A Gaussian-3X Prediction on the Enthalpies of Formation of Chlorinated Phenols and Dibenzo-p-dioxins. Journal of Physical Chemistry A, 2008, 112, 1832-1840.	2.5	19
306	Surface defects in polyelectrolyte multilayers: Effects of drying and deposition cycle. Soft Matter, 2011, 7, 4851.	2.7	19

#	Article	IF	CITATIONS
307	α-MnO2 hollow clews for rechargeable Li-air batteries with improved cyclability. Science Bulletin, 2012, 57, 4210-4214.	1.7	19
308	Coaxial electrospinning fabrication and electrochemical properties of LiFePO4/C/Ag composite hollow nanofibers. Journal of Materials Science: Materials in Electronics, 2013, 24, 4718-4724.	2.2	19
309	Carbonaceous photonic crystals as ultralong cycling anodes for lithium and sodium batteries. Journal of Materials Chemistry A, 2015, 3, 13786-13793.	10.3	19
310	Capillary-bridge–derived particles with negative Gaussian curvature. Proceedings of the National Academy of Sciences of the United States of America, 2015, 112, 2664-2669.	7.1	19
311	Effect of Sc substitution on hydrogen storage properties of Ti–V–Cr–Mn alloys. International Journal of Hydrogen Energy, 2015, 40, 6860-6865.	7.1	19
312	Simple preparation of Cu ₆ Sn ₅ /Sn composites as anode materials for lithium-ion batteries. RSC Advances, 2016, 6, 15279-15285.	3.6	19
313	Graphite felts modified by vertical two-dimensional WO ₃ nanowall arrays: high-performance electrode materials for cerium-based redox flow batteries. Nanoscale, 2018, 10, 10705-10712.	5.6	19
314	Electrolyte Chemistry in 3D Metal Oxide Nanorod Arrays Deciphers Lithium Dendrite-Free Plating/Stripping Behaviors for High-Performance Lithium Batteries. Journal of Physical Chemistry Letters, 2021, 12, 4857-4866.	4.6	19
315	Unraveling the Synergistic Catalytic Effects of TiO ₂ and Pr ₆ O ₁₁ on Superior Dehydrogenation Performances of α-AlH ₃ . ACS Applied Materials & Interfaces, 2021, 13, 26998-27005.	8.0	19
316	A novel adaptive density-based spatial clustering of application with noise based on bird swarm optimization algorithm. Computer Communications, 2021, 174, 205-214.	5.1	19
317	Crystallographic and electrochemical characteristics of Ti45Zr35Ni17Cu3 quasicrystalline alloy ball-milled with nickel powder. Electrochimica Acta, 2006, 51, 3586-3591.	5.2	18
318	Layer-by-layer assembly of single-charged ions with a rigid polyampholyte. Chemical Communications, 2008, , 1741.	4.1	18
319	Hydrogen storage properties of Ti1.4V0.6NiÂ+Âx Mg (xÂ=Â1–3, wt.%) alloys. International Journal of Hydrogen Energy, 2014, 39, 3313-3319.	7.1	18
320	Enhanced electrochemical performance by a three-dimensional interconnected porous nitrogen-doped graphene/carbonized polypyrrole composite for lithium–sulfur batteries. RSC Advances, 2016, 6, 26264-26270.	3.6	18
321	Selecting Appropriate Spatial Scale for Mapping Plastic-Mulched Farmland with Satellite Remote Sensing Imagery. Remote Sensing, 2017, 9, 265.	4.0	18
322	Gaseous sorption and electrochemical properties of rare-earth hydrogen storage alloys and their representative applications: A review of recent progress. Science China Technological Sciences, 2018, 61, 1309-1318.	4.0	18
323	Carbon Supported MoO ₂ Spheres Boosting Ultraâ€Stable Lithium Storage with High Volumetric Density. Energy and Environmental Materials, 2022, 5, 245-252.	12.8	18
324	Microstructures and Properties of Melt-Spun and As-Cast Mg-20Gd Binary Alloy. Journal of Rare Earths, 2006, 24, 466-470.	4.8	17

#	Article	IF	CITATIONS
325	The gas-phase thermochemistry of SeFn, SeFn+, and SeFnâ^' (n=1–6) from Gaussian-3 calculations. International Journal of Mass Spectrometry, 2007, 264, 84-91.	1.5	17
326	The oxidation mechanism of polychlorinated dibenzo-p-dioxins under the atmospheric conditions – A theoretical study. Chemosphere, 2012, 89, 950-956.	8.2	17
327	High temperature performance of La0.6Ce0.4Ni3.45Co0.75Mn0.7Al0.1 hydrogen storage alloy for nickel/metal hydride batteries. International Journal of Hydrogen Energy, 2014, 39, 13231-13239.	7.1	17
328	The atmospheric oxidation mechanism of 2-methylnaphthalene. Physical Chemistry Chemical Physics, 2015, 17, 23413-23422.	2.8	17
329	Novel Signal-Amplified Fenitrothion Electrochemical Assay, Based on Glassy Carbon Electrode Modified with Dispersed Graphene Oxide. Scientific Reports, 2016, 6, 23409.	3.3	17
330	The Influence of Molecular Configuration on the Thermoelectrical Properties of Poly(3-hexylthiophene). Journal of Electronic Materials, 2016, 45, 1389-1396.	2.2	17
331	Bio-inspired self-breathable structure driven by the volumetric effect: an unusual driving force of metal sulfide for high alkaline ion storage capability. Journal of Materials Chemistry A, 2019, 7, 5677-5684.	10.3	17
332	Free-standing 3D nitrogen–carbon anchored Cu nanorod arrays: <i>in situ</i> derivation from a metal–organic framework and strategy to stabilize lithium metal anodes. Journal of Materials Chemistry A, 2020, 8, 1425-1431.	10.3	17
333	Clarifying the nature of the Johari-Goldstein β-relaxation and emphasising its fundamental importance. Philosophical Magazine, 2020, 100, 2596-2613.	1.6	17
334	Initiation of protective autophagy in hepatocytes by gold nanorod core/silver shell nanostructures. Nanoscale, 2020, 12, 6429-6437.	5.6	17
335	Atmospheric oxidation of gaseous anthracene and phenanthrene initiated by OH radicals. Atmospheric Environment, 2020, 234, 117587.	4.1	17
336	Microstructure and crystallization of melt-spun Ti–Ni–Zr–Y alloys. Journal of Alloys and Compounds, 2002, 339, 216-220.	5.5	16
337	Microstructure and mechanical properties of Mg–4Al–4Nd–0.5Zn–0.3Mn alloy. Materials Science & Engineering A: Structural Materials: Properties, Microstructure and Processing, 2009, 515, 98-101.	5.6	16
338	Cations of halogenated methanes: adiabatic ionization energies, potential energy surfaces, and ion fragment appearance energies. Structural Chemistry, 2009, 20, 461-479.	2.0	16
339	Microstructure and electrochemical hydrogen storage characteristics of La0.67Mg0.33â^'xCaxNi2.75Co0.25 (xÂ=Â0–0.15) electrode alloys. International Journal of Hydrogen Energy, 2011, 36, 3050-3055.	7.1	16
340	Electrospinning fabrication and electrochemical properties of LiFePO4/C composite nanofibers. Journal of Materials Science: Materials in Electronics, 2013, 24, 4263-4269.	2.2	16
341	An enzyme-linked chemiluminescent immunoassay developed for detection of Butocarboxim from agricultural products based on monoclonal antibody. Food Chemistry, 2015, 166, 372-379.	8.2	16
342	Advanced Metal Oxide@Carbon Nanotubes for Highâ€Energy Lithiumâ€Ion Full Batteries. Energy Technology, 2018, 6, 766-772.	3.8	16

#	Article	IF	CITATIONS
343	Metal–Organic Coordination Strategy for Obtaining Metalâ€Decorated Moâ€Based Complexes: Multiâ€dimensional Structural Evolution and Highâ€Rate Lithiumâ€Ion Battery Applications. Chemistry - A European Journal, 2019, 25, 8813-8819.	3.3	16
344	Facile synthesis of metal disulfides nanoparticles encapsulated by amorphous carbon composites as high-performance electrode materials for lithium storage. Journal of Alloys and Compounds, 2019, 773, 97-104.	5.5	16
345	Improvement of dehydrogenation performance by adding CeO2 to α-AlH3. International Journal of Hydrogen Energy, 2020, 45, 2119-2126.	7.1	16
346	Structures and electrochemical characteristics of Ti0.26Zr0.07V0.24Mn0.1Ni0.33Mox (x=0–0.1) hydrogen storage alloys. Materials Science and Engineering B: Solid-State Materials for Advanced Technology, 2008, 150, 168-174.	3.5	15
347	Crystallographic and electrochemical characteristics of melt-spun Ti–Zr–Ni–La alloys. Journal of Alloys and Compounds, 2009, 475, 881-884.	5.5	15
348	Facile fabrication of mesoporous N-doped Fe ₃ O ₄ @C nanospheres as superior anodes for Li-ion batteries. RSC Advances, 2014, 4, 713-716.	3.6	15
349	Phase transitions, mechanical properties and electronic structures of novel boron phases under high-pressure: A first-principles study. Scientific Reports, 2014, 4, 6786.	3.3	15
350	A protein extraction method for low protein concentration solutions compatible with the proteomic analysis of rubber particles. Electrophoresis, 2016, 37, 2930-2939.	2.4	15
351	Ti–V–Ni with graphene-mixing icosahedral quasicrystalline composites: Preparation, structure and its application in Ni–MH rechargeable batteries. International Journal of Hydrogen Energy, 2016, 41, 1098-1103.	7.1	15
352	Twist1 in podocytes ameliorates podocyte injury and proteinuria by limiting CCL2-dependent macrophage infiltration. JCI Insight, 2021, 6, .	5.0	15
353	Highly Efficient Hydrogen Storage Capacity of 2.5 wt % Above 0.1 MPa Using Y and Cr Codoped V-Based Alloys. ACS Applied Energy Materials, 2022, 5, 3282-3289.	5.1	15
354	Crystallographic and electrochemical characteristics of Ti45Zr35Ni13Pd7 melt-spun alloys. International Journal of Hydrogen Energy, 2009, 34, 1890-1895.	7.1	14
355	Microstructures and Mechanical Properties of As-Cast and Hot-Rolled Mg-8.43Li-0.353Ymm (Y-riched) Tj ETQq1 I Science, 2012, 43, 709-715.	0.78431 2.2	4 rgBT /Over 14
356	Icosahedral quasicrystalline (Ti1.6V0.4Ni)100â^'xScx alloys: Synthesis, structure and their application in Ni-MH batteries. Journal of Solid State Chemistry, 2013, 202, 1-5.	2.9	14
357	Microwave-assisted hydrothermal synthesis of graphene-wrapped CuO hybrids for lithium ion batteries. RSC Advances, 2014, 4, 51362-51365.	3.6	14
358	Heat shock protein 27 is involved in PCV2 infection in PK-15 cells. Virus Research, 2014, 189, 235-242.	2.2	14
359	The Atmospheric Oxidation Mechanism of Benzyl Alcohol Initiated by OH Radicals: The Addition Channels. ChemPhysChem, 2015, 16, 1542-1550.	2.1	14
360	Pathophysiologic mechanisms of biomedical nanomaterials. Toxicology and Applied Pharmacology, 2016, 299, 30-40.	2.8	14

#	Article	IF	CITATIONS
361	Mechanism of gas-phase ozonolysis of sabinene in the atmosphere. Physical Chemistry Chemical Physics, 2017, 19, 24209-24218.	2.8	14
362	Enhanced electrochemical properties of Ti1.4V0.6Ni with Mo2C or WC coating as negative electrodes for Ni-MH battery. Journal of Alloys and Compounds, 2017, 695, 208-214.	5.5	14
363	Atmospheric oxidation mechansim of polychlorinated biphenyls (PCBs) initiated by OH radicals. Chemosphere, 2020, 240, 124756.	8.2	14
364	Self-catalytic approach to construct graphitized carbon shell for metal oxide: In-situ triggering mechanism and high-performance lithium-ion batteries applications. Journal of Power Sources, 2020, 450, 227631.	7.8	14
365	Carbon Nanotubes Coupled with Metal Ion Diffusion Layers Stabilize Oxide Conversion Reactions in High-Voltage Lithium-Ion Batteries. ACS Applied Materials & Interfaces, 2020, 12, 16276-16285.	8.0	14
366	Equably-dispersed Sb/Sb2O3 nanoparticles in ionic liquid-derived nitrogen-enriched carbon for highly reversible lithium/sodium storage. Electrochimica Acta, 2021, 395, 139210.	5.2	14
367	Icosahedral and Amorphous Phases in Melt-Spun Ti-Zr-Ni-Cu Alloys. Materials Transactions, 2001, 42, 2637-2640.	1.2	13
368	Quinary icosahedral quasicrystalline Ti–V–Ni–Mn–Cr alloy: A novel anode material for Ni-MH rechargeable batteries. Materials Letters, 2011, 65, 2868-2871.	2.6	13
369	Shear Distortion and Failure of Capillary Bridges. Wetting Information Beyond Contact Angle Analysis. Langmuir, 2013, 29, 7776-7781.	3.5	13
370	Ni coated Ti1.4V0.6Ni composite as the negative electrode in Ni–MH battery. Materials Letters, 2015, 161, 686-689.	2.6	13
371	Synthesis of polygonal Co ₃ Sn ₂ nanostructure with enhanced magnetic properties. RSC Advances, 2016, 6, 39818-39822.	3.6	13
372	Effect of MWNTs-addition on cathodic performance of Ti-V-Ni composites for Ni-MH batteries. International Journal of Hydrogen Energy, 2016, 41, 9471-9475.	7.1	13
373	A lateral flow assay for copper(II) utilizing catalytic and stem-loop based signal amplification. Mikrochimica Acta, 2019, 186, 82.	5.0	13
374	Attribution of the land surface temperature response to land-use conversions from bare land. Global and Planetary Change, 2020, 193, 103268.	3.5	13
375	Speech Technology for Unwritten Languages. IEEE/ACM Transactions on Audio Speech and Language Processing, 2020, 28, 964-975.	5.8	13
376	Unraveling the New Role of Metal–Organic Frameworks in Designing Silicon Hollow Nanocages for High-Energy Lithium-Ion Batteries. ACS Applied Materials & Interfaces, 2021, 13, 40471-40480.	8.0	13
377	Encapsulating silicon particles by graphitic carbon enables High-performance Lithium-ion batteries. Journal of Colloid and Interface Science, 2022, 607, 1562-1570.	9.4	13
378	Microstructures and mechanical properties of Mg–2Y–1Mn–1–2Nd alloys fabricated by extrusion. Materials Science & Engineering A: Structural Materials: Properties, Microstructure and Processing, 2010, 527, 4383-4388.	5.6	12

#	Article	IF	CITATIONS
379	Detection of Sulfur Dioxide by Cavity Ring-Down Spectroscopy. Environmental Science & Technology, 2011, 45, 1926-1931.	10.0	12
380	Preparation and characterization of Mg-6Li and Mg-6Li-1Y alloys. Journal of Rare Earths, 2011, 29, 645-649.	4.8	12
381	Effect of Li on structure and electrochemical hydrogen storage properties of Ti55V10Ni35 quasicrystal alloy. International Journal of Hydrogen Energy, 2015, 40, 3015-3022.	7.1	12
382	C ₆₀ (OH) ₂₂ : a potential histone deacetylase inhibitor with anti-angiogenic activity. Nanoscale, 2016, 8, 16332-16339.	5.6	12
383	A splice site mutation in shrunken1-m causes the shrunken 1 mutant phenotype in maize. Plant Growth Regulation, 2017, 83, 429-439.	3.4	12
384	Facile synthesis of nitrogen-doped Sn@NC composites as high-performance anodes for lithium-ion batteries. International Journal of Hydrogen Energy, 2018, 43, 22401-22408.	7.1	12
385	Cerium Oxysulfide with O–Ce–S Bindings for Efficient Adsorption and Conversion of Lithium Polysulfide in Li–S Batteries. Inorganic Chemistry, 2021, 60, 12847-12854.	4.0	12
386	Effect of configuration and conformation on the spin multiplicity in xylylene type biradicals. Science in China Series B: Chemistry, 2000, 43, 524-530.	0.8	11
387	Microstructure and mechanical properties of Mg–12.3Zn–5.8Y–1.4Al alloy. Materials Science & Engineering A: Structural Materials: Properties, Microstructure and Processing, 2008, 485, 55-60.	5.6	11
388	Effect of La–Mg-based alloy addition on structure and electrochemical characteristics of Ti0.10 Zr0.15V0.35Cr0.10Ni0.30 hydrogen storage alloy. International Journal of Hydrogen Energy, 2009, 34, 2646-2653.	7.1	11
389	Effect of zinc and mischmetal on microstructure and mechanical properties of Mg-Al-Mn alloy. Journal of Rare Earths, 2010, 28, 794-797.	4.8	11
390	Coarsening of Silver Nanoparticles in Polyelectrolyte Multilayers. Langmuir, 2013, 29, 11413-11419.	3.5	11
391	Enhanced thermoelectric power and electronic correlations in RuSe2. APL Materials, 2015, 3, .	5.1	11
392	Improved electrochemical performance of Ti1.4V0.6Ni hydrogen storage alloy in its composite with LiAlH4. Journal of Alloys and Compounds, 2017, 724, 1-7.	5.5	11
393	Synthesis of rose-like ZnAl-LDH and its application in zinc–nickel secondary battery. Nanotechnology, 2019, 30, 015602.	2.6	11
394	Pressure Effect on Order–Disorder Ferroelectric Transition in a Hydrogen-Bonded Metal–Organic Framework. Journal of Physical Chemistry Letters, 2020, 11, 9566-9571.	4.6	11
395	Atmospheric oxidation mechanism of acenaphthene initiated by OH radicals. Atmospheric Environment, 2020, 243, 117870.	4.1	11
396	Non-pharmacological treatment for Parkinson disease patients with depression: a meta-analysis of repetitive transcranial magnetic stimulation and cognitive-behavioral treatment. International Journal of Neuroscience, 2021, 131, 411-424.	1.6	11

#	Article	IF	CITATIONS
397	An exploration on the improvement of reversible conversion and capacity retention of Sb2O3-based anode materials for alkali metal-ion storage by Fe-C co-hybridization. Journal of Power Sources, 2021, 506, 230074.	7.8	11
398	Nanoscale localized growth of SnSb for general-purpose high performance alkali (Li, Na, K) ion storage. Chemical Engineering Journal, 2022, 431, 134318.	12.7	11
399	Crystallographic and electrochemical properties of ball-milled quasicrystalline Ti45Zr35Ni17Cu3 alloy with 20mass% Ni. Journal of Alloys and Compounds, 2006, 425, 296-301.	5.5	10
400	Preparation and mechanical properties of a bulk icosahedral quasicrystalline Ti45Zr35Ni17Cu3 alloy. Journal of Non-Crystalline Solids, 2006, 352, 3936-3941.	3.1	10
401	Electrochemical properties of (La1â^xTix)0.67Mg0.33Ni2.75Co0.25 (x=0–0.20, at%) hydrogen storage alloys. Materials Research Bulletin, 2010, 45, 256-261.	5.2	10
402	Oxidation mechanisms of dimethyl selenide and selenoxide in the atmosphere initiated by OH radical. A theoretical study. Chemical Physics, 2011, 382, 98-103.	1.9	10
403	Electrochemical properties of Ti-based Quasicrystal and ZrV2 Laves phase alloy composite materials as negative electrode for Ni–MH secondly batteries. Journal of Non-Crystalline Solids, 2012, 358, 1846-1849.	3.1	10
404	Pressure-induced pseudoatom bonding collapse and isosymmetric phase transition in Zr2Cu: First-principles predictions. Journal of Chemical Physics, 2013, 139, 234504.	3.0	10
405	Effect of LiH on electrochemical hydrogen storage properties of Ti55V10Ni35 quasicrystal. Solid State Sciences, 2016, 52, 19-22.	3.2	10
406	Preparation of a graphitic N-doped multi-walled carbon nanotube composite for lithium–sulfur batteries with long-life and high specific capacity. RSC Advances, 2016, 6, 76568-76574.	3.6	10
407	Multipath colourimetric assay for copper(II) ions utilizing MarR functionalized gold nanoparticles. Scientific Reports, 2017, 7, 41557.	3.3	10
408	Measuring the Efficiency of Energy and Carbon Emissions: A Review of Definitions, Models, and Input-Output Variables. Energies, 2022, 15, 962.	3.1	10
409	Formation and Decomposition of Phenylvinylperoxy Radicals in the Reaction: C6H5C2H2+O2. ChemPhysChem, 2004, 5, 1231-1234.	2.1	9
410	Kinetics of phenyl radical reactions with propane,n-butane,n-hexane, andn-octane: Reactivity of C6H5 toward the secondary C?H bond of alkanes. International Journal of Chemical Kinetics, 2004, 36, 49-56.	1.6	9
411	Quantum Chemistry Study on Cation Structures of Fluorinated and Chlorinated Germanes and Their Radicals. Journal of Physical Chemistry A, 2008, 112, 3454-3465.	2.5	9
412	The Enthalpies of Formation for Polychlorinated Dibenzofurans with Use of G3XMP2 Model Chemistry and Density Functional Theory. Journal of Physical Chemistry A, 2009, 113, 238-245.	2.5	9
413	Gibbs energies of formation of chlorinated benzoic acids and benzoates and application to their reductive dechlorination. Computational and Theoretical Chemistry, 2010, 960, 31-39.	1.5	9
414	Ti1.4V0.6Ni quasicrystal and its composites with xV18Ti15Zr18Ni29Cr5Co7Mn alloy used as negative electrode materials for the nickel–metal hydride (Ni–MH) secondary batteries. Materials Letters, 2012, 79, 122-124.	2.6	9

#	Article	IF	CITATIONS
415	Effect of Ce on electrochemical properties of the TiVNi quasicrystal material as an anode for Ni/MH batteries. International Journal of Hydrogen Energy, 2013, 38, 14810-14815.	7.1	9
416	Preparation and electrochemical performances of LiFePO4/C composite nanobelts via facile electrospinning. Journal of Materials Science: Materials in Electronics, 2014, 25, 1040-1046.	2.2	9
417	First-principles investigations on thermodynamic properties of the ordered and disordered Si0.5Ge0.5 alloys. Applied Physics A: Materials Science and Processing, 2014, 115, 667-670.	2.3	9
418	Wearable non-volatile memory devices based on topological insulator Bi2Se3/Pt fibers. Applied Physics Letters, 2015, 107, .	3.3	9
419	A Meta-Analysis of Open-Path Eddy Covariance Observations of Apparent CO2 Flux in Cold Conditions in FLUXNET. Journal of Atmospheric and Oceanic Technology, 2017, 34, 2475-2487.	1.3	9
420	Hierarchical Molybdenum Dioxide Microflowers Encapsulating Nickel Nanoparticles for Highâ€Performance Lithiumâ€lon Battery Electrodes. ChemElectroChem, 2017, 4, 2915-2920.	3.4	9
421	Gd–Sn alloys and Gd–Sn–graphene composites as anode materials for lithium-ion batteries. New Journal of Chemistry, 2017, 41, 7992-7997.	2.8	9
422	Improved electrochemical hydrogen storage capacity of Ti 45 Zr 38 Ni 17 quasicrystal by addition of ZrH 2. Journal of Materials Science and Technology, 2018, 34, 995-998.	10.7	9
423	Cellular Responses to Exposure to Outdoor Air from the Chinese Spring Festival at the Air–Liquid Interface. Environmental Science & Technology, 2019, 53, 9128-9138.	10.0	9
424	Graphene oxide (GO)-doping SnO ₂ flower-like structure to enhance photocatalytic activity. Fullerenes Nanotubes and Carbon Nanostructures, 2019, 27, 387-394.	2.1	9
425	Impact of Large-Scale Afforestation on Surface Temperature: A Case Study in the Kubuqi Desert, Inner Mongolia Based on the WRF Model. Forests, 2019, 10, 368.	2.1	9
426	Superior reversible hydrogen storage capacity of V-based solid solution alloy above atmospheric pressure with yttrium substitution. Materials Letters, 2021, 297, 129945.	2.6	9
427	Verification of electrolyte decomposition in lithium-ion batteries: Based on the unique bowling-like Sn@C/EG-S composite. Chemical Engineering Journal, 2021, 422, 130520.	12.7	9
428	Excellent kinetics and effective hydrogen storage capacity at low temperature of superlattice rare-earth hydrogen storage alloy by solid-phase treatment. Journal of Physics and Chemistry of Solids, 2022, 161, 110402.	4.0	9
429	Crystallographic and electrochemical characteristics of TiZrNiCu quasicrystal ball-milled with La0.9Zr0.1Ni4.5Al0.5 alloy. Electrochimica Acta, 2007, 52, 3550-3555.	5.2	8
430	Influences of low-Ti substitution for La and Mg on the electrochemical and kinetic characteristics of AB3-type hydrogen storage alloy electrodes. Science China Technological Sciences, 2010, 53, 242-247.	4.0	8
431	Influence of copper addition for silicon–carbon composite as anode materials for lithium ion batteries. RSC Advances, 2016, 6, 56756-56764.	3.6	8
432	Direct Access to Acylated Azobenzenes and Amide Compounds by Reaction of Azoarenes with Benzylic Ethers as Acyl Equivalents. Synthesis, 2016, 48, 1147-1158.	2.3	8

#	Article	IF	CITATIONS
433	RE–Sn (RE = Y, Ce and Gd) alloys as anode materials for lithium-ion batteries. New Journal of Chemistry, 2018, 42, 11525-11529.	2.8	8
434	Ozonolysis of 3-carene in the atmosphere. Formation mechanism of hydroxyl radical and secondary ozonides. Physical Chemistry Chemical Physics, 2019, 21, 8081-8091.	2.8	8
435	Fabrication and electrochemical performance of flower-like ZnAl LDH/SnO2 composites for zinc-nickel secondary batteries. Ionics, 2019, 25, 1715-1724.	2.4	8
436	Crystal reconstruction of binary oxide hexagonal nanoplates: monocrystalline formation mechanism and high rate lithium-ion battery applications. Nanoscale, 2020, 12, 4366-4373.	5.6	8
437	In Situ Growth of Lithiophilic MOF Layer Enabling Dendrite-free Lithium Deposition. IScience, 2020, 23, 101869.	4.1	8
438	Overexpression of an Antisense RNA of Maize Receptor-Like Kinase Gene ZmRLK7 Enlarges the Organ and Seed Size of Transgenic Arabidopsis Plants. Frontiers in Plant Science, 2020, 11, 579120.	3.6	8
439	Size effect of the width of beta-Li phase on the ductility of magnesium–lithium dual-phase alloys. Materials Science & Engineering A: Structural Materials: Properties, Microstructure and Processing, 2021, 814, 141217.	5.6	8
440	Chitosan-based double cross-linked ionic hydrogels as a strain and pressure sensor with broad strain-range and high sensitivity. Journal of Materials Chemistry B, 2022, 10, 3434-3443.	5.8	8
441	Class formation ability and mechanical properties of Ti40Cu40Zr10Ni10 alloy. Journal of Non-Crystalline Solids, 2008, 354, 3653-3658.	3.1	7
442	Theoretical Studies on the Thermochemistry of Stable Closed-Shell C1 and C2 Brominated Hydrocarbons. Journal of Physical Chemistry A, 2008, 112, 4951-4957.	2.5	7
443	Preparation and characterization of As-cast and hot-rolled Mg–3Al–0.5Mn–0.5Zn–1MM alloy. Materials Characterization, 2009, 60, 1507-1511.	4.4	7
444	Self-assembly of anisotropic tobacco mosaic virus nanoparticles on gold substrate. Science China Chemistry, 2011, 54, 137-143.	8.2	7
445	Bond dissociation enthalpies in chlorinated benzenes and phenols and enthalpies of formation of their free radicals: A Gaussian-4 prediction. International Journal of Chemical Kinetics, 2011, 43, 62-69.	1.6	7
446	Evaluation of the catalytic effect of non-noble bismuth on the lead half-cell reaction for lead-based redox flow batteries. RSC Advances, 2016, 6, 56399-56405.	3.6	7
447	Lanthanum Pentafluorobenzoate-Catalyzed Aerobic Oxidative Olefination of Benzylamines with 2-Methylquinoline through Deamination and C–H Bond Functionalization. Synlett, 2016, 27, 2481-2484.	1.8	7
448	In situ synthesis of homogeneous Ce ₂ S ₃ /MoS ₂ composites and their electrochemical performance for lithium ion batteries. RSC Advances, 2017, 7, 6309-6314.	3.6	7
449	Microwave assisted hydrothermal synthesis of Ni 1.5 Co 1.5 S 4 as high-performance electrode material for lithium storage. Applied Surface Science, 2017, 414, 270-276.	6.1	7
450	An enhanced quasicrystalline Ti1.4V0.6Ni alloy electrode modified by uniformly covered RGO for nickel metal hydride battery. Intermetallics, 2020, 127, 106972.	3.9	7

#	Article	IF	CITATIONS
451	The oxidation mechanism of gas-phase ozonolysis of limonene in the atmosphere. Physical Chemistry Chemical Physics, 2021, 23, 9294-9303.	2.8	7
452	Highly Dispersed Antimony–Bismuth Alloy Encapsulated in Carbon Nanofibers for Ultrastable K-Ion Batteries. Journal of Physical Chemistry Letters, 2022, 13, 6587-6596.	4.6	7
453	Pd(OAc) ₂ /PPh ₃ â€Catalyzed Desulfonylative Homocoupling of Arylsulfonyl Chlorides. Chinese Journal of Chemistry, 2015, 33, 535-538.	4.9	6
454	Atmospheric Oxidation Mechanism of Sabinene Initiated by the Hydroxyl Radicals. Journal of Physical Chemistry A, 2018, 122, 8783-8793.	2.5	6
455	Synthesis of Hollow Spherical Zinc-Aluminum Hydrotalcite and Its Application as Zinc Anode Material. Journal of the Electrochemical Society, 2019, 166, A2589-A2596.	2.9	6
456	Significantly improved cycling stability for electrochemical hydrogen storage in Ti1.4V0.6Ni alloy with TiN. Materials Research Bulletin, 2019, 118, 110509.	5.2	6
457	Hydrothermal synthesis of hierarchical flower-like α-CNTs/SnO ₂ architectures with enhanced photocatalytic activity. Fullerenes Nanotubes and Carbon Nanostructures, 2019, 27, 10-13.	2.1	6
458	Different morphologies of strontium carbonate in water/ethylene glycol and their photocatalytic activity. Fullerenes Nanotubes and Carbon Nanostructures, 2019, 27, 46-51.	2.1	6
459	Binder-free layered ZnO@Ni microspheres as advanced anode materials for lithium-ion batteries. Ionics, 2020, 26, 3281-3288.	2.4	6
460	Superior Dehydrogenation Performance of αâ€AlH ₃ Catalyzed by Li ₃ N: Realizing 8.0Âwt.% Capacity at 100 °C. Small, 2022, 18, e2107983.	10.0	6
461	Imidazolium ionic liquids as potential persistent pollutants in aqueous environments: Indirect photochemical degradation kinetics and mechanism. Environmental Research, 2022, 211, 113031.	7.5	6
462	Phase separation and crystallization in a melt-spun Ti45Zr35Ni17Cu3 alloy. Journal of Non-Crystalline Solids, 2008, 354, 1010-1014.	3.1	5
463	The enthalpies of formation of brominated benzenes and phenols: A theoretical prediction. Computational and Theoretical Chemistry, 2010, 957, 72-76.	1.5	5
464	Prediction of gas-phase thermodynamic properties for polychlorinated naphthalenes using G3X model chemistry and density functional theory. Chemosphere, 2010, 78, 77-85.	8.2	5
465	Preparation and wear resistance of Ti–Zr–Ni quasicrystal and polyamide composite materials. Philosophical Magazine, 2011, 91, 2929-2936.	1.6	5
466	Effect of yttrium addition on the formation and mechanical properties of Ti–Zr–Ni–Cu bulk quasicrystalline alloys. Journal of Alloys and Compounds, 2012, 522, 96-100.	5.5	5
467	Synthesis and Characterization of Dibenzo[<i>a</i> , <i>d</i>]cycloheptenâ€5â€one Derivatives for Lightâ€Emitting Diodes. Chinese Journal of Chemistry, 2015, 33, 948-954.	4.9	5
468	Electrochemical hydrogen storage properties of Ti1.4V0.6Ni quasicrystal and TiH composite materials. Journal of Alloys and Compounds, 2015, 630, 158-162.	5.5	5

#	Article	IF	CITATIONS
469	Fabrication of coupled twin-shaped hollow hemispherical calcium molybdate via a facile ultrasound-assisted approach. CrystEngComm, 2015, 17, 2444-2449.	2.6	5
470	â€~Green' immunochromatographic electrochemical biosensor for mercury(II). Mikrochimica Acta, 2016, 183, 2509-2516.	5.0	5
471	Enhanced cycling stability of Ni-MH battery by depositing amorphous carbon film on the Ti1.4V0.6Ni negative electrode. Diamond and Related Materials, 2016, 66, 10-15.	3.9	5
472	Development of an eco-friendly immunochromatographic test strip and its application in detecting Hg ²⁺ without chelators. RSC Advances, 2016, 6, 8729-8735.	3.6	5
473	Fabrication of Ce2S3/MoS2 composites via recrystallization-sulfurization method and their improved electrochemical performance for lithium-ion batteries. Journal of Materials Science: Materials in Electronics, 2017, 28, 12297-12305.	2.2	5
474	Gas-phase ozonolysis of furans, methylfurans, and dimethylfurans in the atmosphere. Physical Chemistry Chemical Physics, 2018, 20, 24735-24743.	2.8	5
475	Crystalline coordination polymer-derived MoS ₂ quantum dot-doped carbon nanoflakes with ultrafast Li ⁺ transfer. Chemical Communications, 2021, 57, 8151-8153.	4.1	5
476	Heterologous expression of ZmGS5 enhances organ size and seed weight by regulating cell expansion in Arabidopsis thaliana. Gene, 2021, 793, 145749.	2.2	5
477	Cellular Uptake, Stability, and Safety of Hollow Carbon Sphere-Protected Fe ₃ O ₄ Nanoparticles. Journal of Nanoscience and Nanotechnology, 2020, 20, 2584-2591.	0.9	5
478	Toward ultra-long cycling stability and high lithium storage performances: Silica anodes with catalytic effects of low-cost metals particles. Applied Materials Today, 2021, 25, 101205.	4.3	5
479	Large-Sized Nickel–Cobalt–Manganese Composite Oxide Agglomerate Anode Material for Long-Life-Span Lithium-Ion Batteries. ACS Applied Energy Materials, 2021, 4, 13811-13818.	5.1	5
480	Crystallographic and electrochemical characteristics of melt-spun Ti-Zr-Ni-Cu alloys. Rare Metals, 2007, 26, 440-444.	7.1	4
481	Effects of rare earth on the structure and properties of Mg–6Zn–5Al–4Gd–1RE (RE = Ce or Y) alloys. Journal of Materials Research, 2008, 23, 2609-2621.	2.6	4
482	Refinement of edge-to-edge matching model and its application in the Mg17Al12/α-Mg and α-Y/α-Mg systems. Intermetallics, 2009, 17, 104-108.	3.9	4
483	Study on information extraction of rape acreage based on TM remote sensing image. , 2011, , .		4
484	Electrochemical hydrogen storage properties of non-stoichiometric La0.7Mg0.3â^'xCaxNi2.8Co0.5 (x=0–0.10) electrode alloys. Journal of Alloys and Compounds, 2011, 509, 5280-5284.	5.5	4
485	A composite based on Fe substituted TiVNi alloy: Synthesis, structure and electrochemical hydrogen storage property. Intermetallics, 2013, 34, 18-22.	3.9	4
486	Synthesis of single-crystalline LiFePO4 with rhombus-like morphology. Ionics, 2015, 21, 295-299.	2.4	4

#	Article	IF	CITATIONS
487	Effect of Li on electrochemical properties of Ti1.4V0.6Ni quasicrystal alloy produced by rapid quenching. Intermetallics, 2015, 62, 50-55.	3.9	4
488	Effect of Li atom infiltration by the way of electro-osmosis on electrochemical properties of amorphous Mg65Ni27La8 alloy used as negative electrode materials for the nickel–metal hydride secondary batteries. Journal of Non-Crystalline Solids, 2015, 415, 30-35.	3.1	4
489	Concentric nano rings observed on Al-Cu-Fe microspheres. Applied Physics Letters, 2016, 108, 223105.	3.3	4
490	Quantitative Security Assessment Method based on Entropy for Moving Target Defense. , 2017, , .		4
491	Graphene oxide (GO) doped CeO ₂ as potential enhancer of methyl orange degradation. Fullerenes Nanotubes and Carbon Nanostructures, 2019, 27, 344-350.	2.1	4
492	Theoretical assessment of wettability on silane coatings: from hydrophilic to hydrophobic. Physical Chemistry Chemical Physics, 2019, 21, 8257-8263.	2.8	4
493	A Different Silica Surface: Radical Oxidation of Poly(methylsilsesquioxane) Thin Films and Particles (Tospearl). Langmuir, 2020, 36, 10110-10119.	3.5	4
494	High-rate lithium/sodium storage capacities of nitrogen-enriched porous antimony composite prepared from organic-inorganic ligands. Applied Surface Science, 2021, 563, 150297.	6.1	4
495	Structure and Electrochemical Performance of Al and Y Co-Doped α-Nickel Hydroxide as a Cathode for a Ni-MH Battery. Energy & Fuels, 2021, 35, 19835-19842.	5.1	4
496	Numerical Analysis of High-Velocity Oxygen Fuel Thermal-Spray Process for Fe-Based Amorphous Coatings. Coatings, 2021, 11, 1533.	2.6	4
497	Electrolytic Deposition and Diffusion of Lithium onto Magnesium-9ÂWtÂPct Yttrium Bulk Alloy in Low-Temperature Molten Salt of Lithium Chloride and Potassium Chloride. Metallurgical and Materials Transactions B: Process Metallurgy and Materials Processing Science, 2009, 40, 779-784.	2.1	3
498	Strings of interconnected hollow carbon nanoparticles with porous shells prepared using simple solid-phase synthesis. Materials Science and Engineering B: Solid-State Materials for Advanced Technology, 2009, 158, 79-81.	3.5	3
499	Development and analytical validation of an Enzyme-Linked Immunosorbent Assay (ELISA) for the detection of copper in human hair and serum samples. Analytical Methods, 2013, 5, 2578.	2.7	3
500	Solid Electrolytes: Na3PSe4: A Novel Chalcogenide Solid Electrolyte with High Ionic Conductivity (Adv. Energy Mater. 24/2015). Advanced Energy Materials, 2015, 5, .	19.5	3
501	Electrochemical hydrogen storage properties of TixV65â^'xNi35 (x=45, 55) alloys produced by rapid-quenching. Materials Letters, 2015, 141, 291-293.	2.6	3
502	Oneâ€step synthesis of novel flowerâ€like Snâ€doped ZnO architectures with enhanced photocatalytic activity. Surface and Interface Analysis, 2020, 52, 91-97.	1.8	3
503	Superior electrochemical characteristics of A2B7-type hydrogen storage alloy at ultralow temperature with the addition of alane. Journal of Materials Science, 2021, 56, 8159-8171.	3.7	3
504	A Rare Autosomal Dominant Variant in Regulator of Calcineurin Type 1 (RCAN1) Gene Confers Enhanced Calcineurin Activity and May Cause FSGS. Journal of the American Society of Nephrology: JASN, 2021, 32, 1682-1695.	6.1	3

#	Article	IF	CITATIONS
505	Signal-Amplified Lateral Flow Test Strip for Visual Detection of Cu2+. PLoS ONE, 2017, 12, e0169345.	2.5	3
506	Manganese coating α-Ni(OH)2 as high-performance cathode material for Ni-MH battery. Ionics, 2022, 28, 1265-1272.	2.4	3
507	Market Integration and Price Dynamics under Market Shocks in European Union Internal and External Cheese Export Markets. Foods, 2022, 11, 692.	4.3	3
508	Microstructure and strengthening mechanism of die-cast Mg–Gd based alloys. Journal of Materials Research, 2008, 23, 1269-1275.	2.6	2
509	A Highly Efficient and Environmentally Friendly CMCâ€Supported Lanthanide Catalyst for Oneâ€pot Synthesis of Substituted Imidazoles. Chinese Journal of Chemistry, 2009, 27, 343-346.	4.9	2
510	Potential energy surfaces for protonation of hydrochlorofluoromethanes. Computational and Theoretical Chemistry, 2009, 913, 240-246.	1.5	2
511	Electrochemical Codeposition of Magnesium-Based Alloys from Dimethylformamide Solutions at Room Temperature. Electrochemical and Solid-State Letters, 2010, 13, D15.	2.2	2
512	Structures and energetics of SiGeHz0,+1, Ge2Hz0,+1, and Si2Hz0,+1: A systematic theoretical study. International Journal of Mass Spectrometry, 2012, 311, 56-63.	1.5	2
513	Investigation on the Structure and Electrochemical Properties of La-Ce-Mg-Al-Ni Hydrogen Storage Alloy. Journal of Chemistry, 2013, 2013, 1-6.	1.9	2
514	Impact of pH on Morphology and Electrochemical Performance of LiFePO4as Cathode for Lithium-ion Batteries. Integrated Ferroelectrics, 2015, 164, 98-102.	0.7	2
515	Micellization of 4-Hydroxynaphthalimides: The Solvent-induced Aggregation and the Detection of Low-level Water in THF. Chemistry Letters, 2016, 45, 1162-1164.	1.3	2
516	Synthesis, Surface Activity, and Antimicrobial Efficacy of Hydrogenated Cardanolâ€Đerived Positively Charged Asymmetric Gemini Surfactants. Journal of Surfactants and Detergents, 2019, 22, 1289-1298.	2.1	2
517	Photochemical transformation of pyridinium ionic liquids in aqueous phase: Kinetics, products and mechanism. Journal of Environmental Chemical Engineering, 2021, 9, 106638.	6.7	2
518	Preparation and transport properties of a bulk icosahedral quasicrystalline Ti45Zr35Ni17Cu3 alloy. Physica B: Condensed Matter, 2007, 393, 316-320.	2.7	1
519	Selective Separation of Cd(II) Ion from Aqueous Solution by Cd(II)-Imprinted Polymers. , 2009, , .		1
520	Effect of La on the crystalline and electrochemical properties of Ti-Zr-Ni melt-spun alloys. Rare Metals, 2009, 28, 333-337.	7.1	1
521	ELECTROCHEMICAL DEPOSITION OF MAGNESIUM IN ETHEREAL GRIGNARD SALT SOLUTION WITH IONIC LIQUID ADDITIVE. International Journal of Modern Physics B, 2009, 23, 838-842.	2.0	1
522	Synthesis and characterization of ZnO–In2O3 junction structure. Materials Letters, 2011, 65, 113-115.	2.6	1

#	Article	IF	CITATIONS
523	Influence of Sc on Microstructure and Mechanical Properties of High Zn-Containing Mg Alloy. Advances in Materials Science and Engineering, 2014, 2014, 1-5.	1.8	1
524	Light-activated mesoporous nanocarriers to overcome drug resistance of cancer cells. Nanomedicine: Nanotechnology, Biology, and Medicine, 2016, 12, 519.	3.3	1
525	Recovery Phenomenon During Annealing of an As-Rapidly Solidified Al Alloy. Metallurgical and Materials Transactions A: Physical Metallurgy and Materials Science, 2017, 48, 3027-3035.	2.2	1
526	Synthesis, Surface Activity, and Antimicrobial Efficacy of Diaryliodonium Saltâ€Derived Amphiphiles. Journal of Surfactants and Detergents, 2018, 21, 323-334.	2.1	1
527	Mechanism and fate of cyclohexadienyl radicals with O2 in the atmosphere. A theoretical study. Chemical Physics Letters, 2018, 707, 172-177.	2.6	1
528	Self-Assembly of Monodispersed Closely Packed Composite Superstructures by Anchoring Nanoparticles into Multihierarchical Frameworks. ACS Sustainable Chemistry and Engineering, 2020, 8, 18966-18974.	6.7	1
529	Multimodal Word Discovery and Retrieval With Spoken Descriptions and Visual Concepts. IEEE/ACM Transactions on Audio Speech and Language Processing, 2020, 28, 1560-1573.	5.8	1
530	Competitive immune-nanoplatforms with positive readout for the rapid detection of imidacloprid using gold nanoparticles. Mikrochimica Acta, 2021, 188, 356.	5.0	1
531	MICROSTRUCTURE AND MECHANICAL PROPERTIES OF TI-BASED METALLIC GLASS MATRIX COMPOSITES. International Journal of Modern Physics B, 2009, 23, 1260-1264.	2.0	0
532	Effect of AB5 alloy on Ti0.10Zr0.15V0.35Cr0.10Ni0.30 hydrogen storage alloy. Journal of Applied Electrochemistry, 2009, 39, 1565-1572.	2.9	0
533	Joint block motion estimation in H.264/AVC. , 2009, , .		Ο
534	Grain refinement and mechanism of CAl0.5W0.5 compound in Mg-Al alloys. Rare Metals, 2010, 29, 630-634.	7.1	0
535	Electrochemical hydrogen storage characteristics of TiVNi-quasicrystalline composite materials. International Journal of Nanotechnology, 2013, 10, 80.	0.2	0
536	Electrochemical Hydrogen Storage Properties of Sintered La0.7Mg0.3Ni2.5Co0.4Mn0.2Al0.1 Alloy. Asian Journal of Chemistry, 2013, 25, 4825-4827.	0.3	0
537	Extraction of Metastable Icosahedral Quasicrystalline Nanoparticles from Zirconium and Hafnium Based Metallic Glasses. Microscopy and Microanalysis, 2014, 20, 1484-1485.	0.4	0
538	Characterization of Sphere-like Structure in Aluminum based Alloy. Microscopy and Microanalysis, 2016, 22, 2016-2017.	0.4	0
539	Application of GF-1 data in agricultural monitoring in China. , 2016, , .		0
540	Microstructure evolution and mechanical properties of Zr–45Ti–5Al–3V alloy processed by electric field-assisted extrusion. Journal of Materials Research, 2016, 31, 3580-3587.	2.6	0

#	Article	IF	CITATIONS
541	Highly degrade RhB solution ability based on CNTs-doped flower-like ZnO material. Fullerenes Nanotubes and Carbon Nanostructures, 2019, 27, 934-938.	2.1	Ο
542	Facile synthesis of hierarchical hexagonal flower-like WO3·0.33H2O nanostructures with enhanced visible-light-driven photocatalytic activity. Fullerenes Nanotubes and Carbon Nanostructures, 2019, 27, 755-761.	2.1	0
543	Fatty Acid Quaternary Ammonium Surfactants Based on Renewable Resources as a Leveler for Copper Electroplating. ChemElectroChem, 2019, 6, 3213-3213.	3.4	0
544	Synthesis of Ce-doped GN/ZnO architectures with enhanced photocatalytic activity. Fullerenes Nanotubes and Carbon Nanostructures, 2019, 27, 28-32.	2.1	0
545	Effects of silicon on the growth, nutrient uptake and cadmium accumulation of tomato seedlings. International Journal of Environmental Analytical Chemistry, 0, , 1-14.	3.3	0
546	Effects of Gd on the microstructure and mechanical properties of Mg–Li dual-phase alloys. International Journal of Materials Research, 2020, 111, 432-438.	0.3	0